Title
NUCLEAR COLLISIONS AT HIGH ENERGIES

Authors
Nagamiya, S.
Randrup, J.
Symons, T.J.M.

Publication Date
1984

LBL-17332
Preprint

Lawrence Berkeley Laboratory
UNIVERSITY OF CALIFORNIA

Submitted to Annual Review of Nuclear and
Particle Science

NUCLEAR COLLISIONS AT HIGH ENERGIES

S. Nagamiya, J. Randrup, and T.J.M. Symons

January 1984

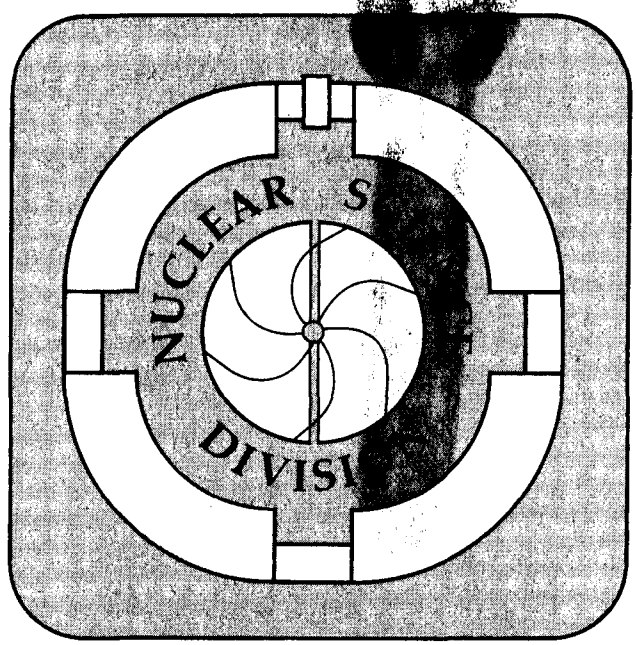

Prepared for the U.S. Department of Energy under Contract DE-AC03-76SF00098

DISCLAIMER

LBL - 17332

NUCLEAR COLLISIONS AT HIGH ENERGIES*

S. Nagamiya

Department of Physics, Faculty of Science,
University of Tokyo, Hongo, Bunkyo-ku, Tokyo 113, Japan

J. Randrup and T. J. M. Symons

Nuclear Science Division, Lawrence Berkeley Laboratory,
University of California, Berkeley, CA 94720

January 1984

*This work was supported by the Director, Office of Energy Research, Division of Nuclear Physics of the Office of High Energy and Nuclear Physics of the U.S. Department of Energy under Contract DE-AC03-76SF00098.

CONTENTS

1. INTRODUCTION

In 1972, the first nuclear beams were accelerated to relativistic energies in synchrotrons at Berkeley and Princeton, ushering in a new field of study for nuclear physicists. At that time the possibility of producing hot, highly compressed nuclear matter offered great promise for extending our knowledge of the nuclear equation of state away from the equilibrium found in finite nuclei. Ten years later, this remains the principal goal of the field although progress in this particular direction has been slow. This does not mean, however, that the developing field of high energy nuclear collisions has moved slowly. Great progress has been made in our understanding of nuclear collisions and results have been found that are intrinsically interesting and will also be invaluable for planning new experiments at higher energies. In this article, we review the progress that has been made in understanding these processes and give some indications of the directions in which the field appears to be heading.

We should emphasize that this is an experimental review. Models will be introduced as needed to aid in interpretation and correlation of the data, but we hardly touch upon the considerable theoretical work concerning potential knowledge that may be gained from high energy collisions in the future. Thus, the reader will find discussions of hydrodynamics or the abrasion-ablation model but should not expect to learn in detail about pion condensates, Lee-Wick matter or the quark-gluon plasma. We have restricted our discussion to data from collisions between heavy ($A>4$) nuclei at beam energies up to a few A GeV. High energy

hadron-nucleus collisions have been left out as have the exciting new experiments at the CERN ISR on collisions of ultra-relativistic light ions. Even within our restricted field, we have had to make difficult choices and some important topics, such as target fragmentation and the study of anomalons, are not considered.

Before starting this detailed survey, we should like to make some general introductory remarks. In nuclear reactions at beam energies above a few 100 A MeV the available energy is much greater than the nuclear binding energy, so that the collisions are quite dramatic in comparison to those at low energy. This is illustrated vividly in Figure 1 which displays an emulsion recording of such a collision (1). The multiplicity of product particles is large and the kinematic domain into which they are emitted is very wide. This is partly due to the larger phase space available at high beam energies and partly to the fact that the reaction mechanism is basically different from that of low energy nuclear collisions. In ordinary nuclear matter the density of nucleons is around $\rho_0 \approx 0.16$ fm^{-3} so that the typical closest-neighbor separation is ≈ 2 fm. This distance is larger than the de Broglie wavelength of a nucleon moving with a kinetic energy above a few hundred MeV. Therefore, at such energies, the projectile nucleons can recognize the individuality of the target nucleons (and vice versa). At the same energies, the mean free path λ of a nucleon moving through normal nuclear matter approaches the "free" value $\lambda_0 = 1/(\rho_0 \sigma_{NN}) \approx 1.6$ fm (where σ_{NN} is the nucleon-nucleon interaction cross section which is fairly constant at high energies). This value is smaller than the nuclear radius $R_A \approx 1.2\ A^{1/3}$fm $\approx$ 3-7 fm. Furthermore, the diferential cross section

grows predominantly forward peaked. Consequently, an incident high-energy nucleon will typically experience a sequence of several collisions with the target nucleons while tending to preserve its forward motion.

As it has turned out, it is possible to understand many of the main features of high-energy nuclear collisions on a very simple conceptual basis in which the colliding nuclei are pictured as two clouds of individual nucleons which propagate through each other with the nucleons suffering sequential hard collisions with those of the other nucleus (see Figure 2). While certainly simplistic, and in many ways inadequate, this picture serves to introduce some concepts which have proven very useful in organizing and discussing the various characteristic features of these processes. In particular, the concept of participants and spectators follows naturally from this picture (2,3). In a typical collision, such as the one depicted in Figure 2, the outer parts of the two nuclei will miss and the nucleons in them will not experience violent interactions; these parts are denoted the projectile and target spectators, respectively. The remaining two parts interpenetrate and their nucleons suffer several hard collisions; these particles are called the participants. [For the empirical validity of this picture see refs.(4,5).]

The state of motion of a particle with mass m, momentum $\vec{p} = (\vec{p}_\perp, p_\parallel)$ and energy E can conveniently be characterized by the dimensionless rapidity vector $\vec{y} = (\vec{p}_\perp/mc,\ y)$ where $y = \text{atanh}(p_\parallel c/E)$ is the ordinary rapidity. ($p_\parallel$ denotes the momentum component along the beam and $\vec{p}_\perp$ is the transverse momentum.) Since $\vec{y}$ is additive under Lorentz boosts along the beam, contour plots of the invariant differential cross section $Ed\sigma/d\vec{p} \sim d\sigma/d\vec{y}$ remain undistorted under such transformations. In the

non-relativistic limit $\vec{y}$ is simply the velocity $\vec{v}$ divided by c.

The spectator matter, which has suffered only little disturbance through the collision, will then emerge with rapidities close to those of the respective initial nuclei, y_p and y_T. This matter will remain rather cold so that fairly large fragments may result. Since the spectators are characterized by the neutron-to-proton ratio associated with their respective primogenitors, the resulting frgments will tend to carry the same ratio and thus ordinarily be excessively neutron rich for their mass. This special feature of a high-energy nuclear collision can be turned into a very powerful means of producing neutron rich nuclei far from the stability line. This topic will be discussed in Section 4.

The fate of the participant portion of the collision system is more complicated. The nucleons will suffer hard collisions as the two nucleon clouds interpenetrate. These collisions may excite some of the nucleons, mostly into Δ resonances, and mesons are produced. Later on, as the system disassembles, the longer-range interactions between the emerging particles are important for the formation of the final fragments. Clearly, the first important task is to understand the dynamics of such multiple collisions. Summarizing our basic knowledge of this will occupy Section 2.

There are many systems in nature where microscopic descriptions such as the one we have just described are unnecessarily cumbersome. For example, in studying the behavior of gases, one does not need to follow the fate of individual gas molecules in order to learn how a gas will behave under variation of temperature and pressure; one only needs to know the macroscopic equation of state. Theoretically, various expectations

for matter at high density and temperature have been proposed as the highlights of high energy nuclear collisions; pion condensation (6,7), abnormal nuclear matter (8,9), and quark matter (10), as shown in Figure 4. Matter at high density and temperature is a new domain in nuclear physics, since until now we have been restricted to the region of densities around ρ_0 and temperatures up to 10-20 MeV. An important caveat, however, is that the system formed must be large enough and live long enough for such a description to be valid. Experimental efforts towards this goal will be discussed in Section 3.

Recently, very heavy nuclear beams, such as ^{139}La and ^{238}U, have become available at the Bevalac in Berkeley and the field of high-energy nuclear collisions is growing rapidly. Currently, planning is under way for the construction of accelerators to provide nuclear beams at ultrarelativistic energies. We hope that the present review may serve to give a quick impression of the major accomplishments so far and also be helpful in planning for the future.

2. LIGHT-PARTICLE EMISSION AT LARGE ANGLES

2.1 Energy and Angular Distributions

Energy and angular distributions of protons produced in nearly equal-mass collisions at beam energies of 800 A MeV (11) are plotted in Figure 4. The c.m. 90° energy distributions are selected, because at this angle the contribution from spectators should be the smallest, as expected from the participant-spectator picture shown in Figure 2. The spectral shapes are nearly identical for all the cases, implying that the beam energy per nucleon, rather than the total beam energy, determines the basic dynamics of proton emission. A "shoulder-arm" type spectrum shape is observed with an approximately exponential form in the high-energy region,

$$E \frac{d\sigma}{d\vec{p}} \quad \alpha \quad \exp\left(-E^{c.m.}/E_0\right) \qquad (1)$$

In particular, a copious production of high-energy protons is observed in the region far beyond the free NN kinematical limit (≃ 182 MeV in this case). Even if a proper Fermi motion is included (12), the production of these high-energy protons cannot be explained by a model in which a nucleon suffers at most a single one NN collision. Finally, the angular distribution shows strong forward and backward peakings in the c.m. frame.

Historically, these data were discussed first with a fireball model (13-17) which assumes that the total available energy of the participants is completely thermalized. The size of the fireball is given by the geometric clean cut separation into participants and spectators. While the overall proton yields are fairly well accounted for, this model has various difficulties in explaining the data. First, it predicts a pure

exponential shape in the entire kinematic region, which conflicts with the shoulder-arm shape. Secondly, the predicted angular distribution is isotropic in the c.m. frame of the fireball, in contrast to the observed angular anisotropy shown in Figure 4.

In order to explain the angular anisotropy, two modified thermal models, the firestreak model (18,19) and the two-fireball model (20), were introduced. The firestreak model assumes that the participant regions are divided into many tubes along the beam direction and thermal equilibrium is assumed in each pair of juxtaposed tubes. The cross section is then given by an incoherent sum of these completely inelastic tube-tube collisions. The two-fireball model introduces the concept of nuclear transparency by assuming that only part of the available energy goes to thermal motion with the rest remaining in translational motion. Both models qualitatively explain the observed large angular anisotropy, but still fail to reproduce the shoulder-arm shape.

In order to make progress on this problem it is useful to also consider the pions. Pion spectra show an almost pure exponential shape (11), but the observed slope $E_0(\pi)$ is systematically smaller than $E_0(p)$. This difference cannot be explained in the thermal model which assumes that both protons and pions are emitted from a common source so that they should be characterized by the same temperature.

This puzzle led to a modified thermal model called the thermal explosion model (21). It assumes that the system dissassembles in an explosive manner with a radially expanding flow superposed on the chaotic thermal motion. Since heavy, slow particles (nucleons) are affected more by this flow than light, fast ones (pions), the spectral shape for protons

deviates substantially from exponential in the low-energy region, and is quite similar to the observed shoulder-arm shape. Furthermore, the model also reproduces the observed slope difference between protons and pions for the same reason. However, this model cannot explain the angular anisotropy.

The various characteristic features of the data can also be fairly well understood in the microscopic intranuclear cascade picture outlined in the introduction and illustrated in Figure 2. While several elaborate implementations of this general picture have been made and employed (22-29) the main results can be understood in the simple linear-cascade or "rows-on-rows" approximation in which a given nucleon only collides with its juxtaposed partners in the other nucleus (12,30,31). In this model high-energy particles result from multiple NN collisions and are in approximate agreement with the thermal results. Furthermore, the low energy part of the spectrum results in large part from single quasi-elastic NN collisions which yield a peak at $E_p^{c.m.} \simeq E_{Beam}^{c.m.}/A \simeq 182$ MeV in the present case, thus producing the shoulder-arm feature. Finally, the angular anisotropy emerges naturally due to the different velocities of the various row-row systems, just as in the firestreak model.

A simple model bridging the microscopic rows-on-rows model and the macroscopic firestreak model is the phase-space model (32,33). It assumes that statistical equilibrium is reached in each row-row system separately. Thus the model can be considered a generalization of the firestreak model to take account of the finite supply of nucleons and energy in each row-row system. In addition to reproducing the spectral

shoulder-arm shape and the anisotropy, this model also predicts pions to be colder than nucleons, due to the energy expended in producing the pion.

Recently, data for K^+ production with 2.1 A GeV Ne beams have been reported (34), as shown in Figure 5. The spectrum shape is again exponential with the inverse slope of $E_0 \simeq 142$ MeV, which is larger than E_0 for protons and pions, satisfying the relationship

$$E_0(\pi) < E_0\ (p) < E_0\ (K^+). \qquad (2)$$

This is at variance with both the phase-space and thermal-explosion models. [The former yields $E_0(K^+) < E_0(\pi) < E_0(p)$ because the threshold energy for K^+ production is much higher than that for π production (35,36), whereas the latter yields $E_0(\pi) < E_0(K^+) < E_0(p)$ because $m_\pi < m_{K^+} < m_p$.]

A simple argument for the above observation (Eq. 2) has been made in terms of the mean free paths of the product particles (37). The energy density of the system reaches a maximum value at a certain time at which point mesons are expected to be created most copiously. Subsequently the system expands and cools. Since particles with a long mean free path would escape more easily from the system, they would reflect the earlier hot stage of the collision by carrying higher kinetic energies, hence a larger value of E_0. Since the value of the mean free path λ satisfies the relation of $\lambda(\pi) < \lambda(p) < \lambda(K^+)$ in nuclear matter, we expect the above relation (2).

Calculations of K^+ production have been made both within the microscopic framework (35,38-40) and within the thermal framework (36,41-43). In view of the small elementary kaon production cross sections one would not expect the establishment of chemical equilibrium during the rather short reaction time and indeed the thermal models overpredict the K^+ yields substantially. Contrary to this, the microscopic calculations reproduce the K^+ yield very well. However, they tend to give fairly cold kaons. This is at variance with the data which show rather substantial yields at high energies. A possible mechanism for this feature was suggested to be the elastic scattering of the produced kaons off the surrounding fast-moving nucleons (38). Calculations including the contribution from pion-nucleon interactions to produce K^+ further improve the agreement with the data although certain deviations still remain (39,40,43).

Before finishing this section, it is worthwhile to mention recent data on proton energy distributions at c.m. 90° in 800 A MeV C + C collisions (44). Data are shown in Figure 6, which cover invariant cross sections over eight orders of magnitude. The data show downward deviation from the exponential shape not only below 200 MeV but also above 700 MeV, most likely due to the limited phase space for emission of high-energy protons. Cascade calculations (27,28) lead to a slope steeper than the data in the high-energy region, which may suggest that some mechanism other than simple multiple NN collisions is at work.

2.2 Large-Angle Two-Particle Correlations

Measurements of two-particle correlations further clarify the reaction

mechanism. The in-plane to out-of-plane coincidence ratio for two protons has been measured in 800 A MeV C + C collisions (45,46). Here, the first proton was detected at a fixed angle, $\theta^{Lab} = 40^{\circ}$ and the angular distribution of this ratio was measured as a function of the angle of the second proton. As shown in Figure 7, the ratio is larger than unity for C + C and it peaks at $\theta = 40^{\circ}$, implying that two protons tend to be emitted at $\theta_1 = \theta_2 = 40^{\circ}$ on opposite sides, as illustrated in the upper right corner. These kinematics are exactly what we expect from pp quasi-elastic scattering (pp QES), and therefore, the data show the existence of the direct knock-out component in high-energy nuclear collisions. From detailed analysis of the peak height it was estimated that in C + C collisions at $E^{Lab}_{Beam} = 800$ A MeV, about 40% of protons emitted at $E_p^{c.m.} \simeq 182$ MeV experience only a single NN collision.

Roughly speaking, the probability that a nucleon does not suffer an additional collision after the first one is given by $\exp(-R/\lambda)$, where λ and R are, respectively, the mean free path and the radius of the interaction zone. For C + C collisions, the estimated value of R, based on the participant-spectator model, is about 2 fm. On the other hand, recent experiments determined the value of λ to be 2.4 fm at 800 MeV (47). Therefore, we have $\exp(-R/\lambda) \simeq 0.4$, which is in agreement with the data. This number also agrees with several theoretical calculations (26,31,32,48,49). In addition, this result supports the intuitive expectation, described in Section 1, that a nuclear collision at high energy consists mostly of hard NN collisions, not only single but also multiple, because, even in light-mass systems, more than half the nucleons experience at least two hard NN collisions.

For Ar + Pb collisions the angular distribution of the coincidence ratio shows a completely different pattern from that observed for C + C collisions, as seen from Figure 7. The ratio is smaller than unity at small angles ($\theta < 70^\circ$). This was first ascribed to nuclear shadowing, as illustrated in the lower right corner (45,46). However, the observation of ratios larger than unity at large angles ($\theta > 80^\circ$) cannot be explained by this mechanism. This puzzle will be discussed later in Sec. 3.3.

2.3 Composite Fragments

Particles emitted from the participant region are mainly single nucleons and, to some extent, single pions. This is expected since the energy transfers in the primary hard NN collisions are large in comparison with typical nucleon separation energies and often also large enough to produce a pion. There is, however, also a significant yield of light composite nuclear fragments, especially d, t, ^{3}He, and α.

It has been found that the spectral shapes of the light composite fragments are related by a simple power law to the observed proton spectra (11,50,51),

$$[E(\frac{d\sigma}{d\vec{p}})]_A = C_A\left\{[E(\frac{d\sigma}{d\vec{p}})]_p\right\}^A \qquad (3)$$

for $\vec{p}_A = A\,\vec{p}_p$. This feature is illustrated in Figure 8.

A simple interpretation of the above relationship has been made in terms of a coalescence model (50-54), according to which primordial nucleons produced sufficiently close in momentum space may coalesce into a composite fragment due to their final-state interactions. In such a

picture, the probability for observing a deuteron with a specified velocity is proportional to the product of the probabilities for having a neutron and a protron with that same velocity. Since the primordial neutron spectra are expected to be nearly proportional to the proton spectra the above relation (Eq. (3)) follows, with the normalization constant C_A being adjustable for each fragment species. It should be noted, though, that the coalescence model relates the observed composite spectra to the primordial proton spectra while the empirical relation is between observed spectra only. When the local composite yield is small in comparison with the local proton yield there is little difference between primordial and observed proton yields. But there are cases where this perturbation condition is not met (55). This fact cast some doubt on the general validity of the coalescence picture.

An alternate framework for discussing the yield of composite fragments is the chemical equilibrium model (16,17,56,57). In this picture, the participant source is considered as a gas of fragments in thermal and chemical equilibrium. The ensuing rate equations determining the equilibrium species composition then lead to relations of the form of Eq. (3) between the observed spectral shapes. This fact would seem to favor the chemical equilibrium model. However, the model predictions of the relative yields are too large by nearly an order of magnitude (58). Thus the mechanism of composite fragment formation is still not well understood.

Recently, systematic studies of the d/p ratio as a function of event multiplicity have been performed by the LBL-GSI group (59) at the Bevalac, using a multi-detector device called the Plastic Ball/Wall

(60). Typical results are shown in Figure 9. As event multiplicity increases, the d/p ratio increases as well. This is understood as due to the finite size of the fragments (59,61). Accordingly, the ratio approaches a constant at high multiplicities and only in this regime can thermal models be properly applied. However, a quantitative comparison has not yet been made.

Since the d/p ratio can be related to the phase-space density in the source, it has been noted (62) that the specific entropy S can be extracted by the use of the relation $S = 3.95 - \ln (d/p)$. The inherent assumption of isentropic disassembly is supported by various theories (21, 63-65). Thus, a measurement of S would probe the entropy associated with the initial hot stage of the collision. However, the validity of the above simple relation has since been questioned (66) and, furthermore, it has been demonstrated that the observed d/p ratio can be quite different from the primordial value, due to the break-up of unstable fragments (67). Consequently, the question of entropy production is still wide open.

3. SEARCH FOR NEW FORMS OF MATTER

3.1 Efforts to Probe Density and Temperature

In order to elucidate the extent to which nuclear matter is compressed or heated up during the course of a nuclear collision, we now discuss attempts to deduce the density and temperature experimentally.

Concerning the density, ρ, if we measure both the multiplicity of nucleons emitted from the interaction region, m_N, and its volume, V, then we can extract it from the relation $\rho = m_N/V$. Since the measurement of m_N is rather straightforward (for charged particles at least), the question is how to determine the source volume. We recall that stellar radii can be measured by $\gamma\gamma$ interferometry, exploiting the Hanbury-Brown/Twiss effect (68). This idea was applied to high-energy collisions for the purpose of determining the size of the interaction region (69-71) using identical pions rather than photons. Assume that particles are emitted statistically from a source with a certain space-time structure $\rho(\vec{r},t)$. The quantum correlations between two identical particles emitted from the source then produce a structure in the observed two-particle cross section $d^2\sigma(\vec{p}_1,\vec{p}_2)/d\vec{p}_1 d\vec{p}_2$, where $\vec{p}_1$ and $\vec{p}_2$ are the momenta of the two particles. The scale of this structure reflects the space-time extension of the source via the uncertainty relation. Specifically, if the source $\rho(\vec{r},t)$ is assumed to be a Gaussian characterized by the radius R and life-time τ, then, for identical bosons, the enhancement in the two-particle counting rate relative to the product of the two one-particle counting rates is given by (72,73)

$$C_2 = \sigma_0 \frac{d^2\sigma(\vec{p}_1,\vec{p}_2)\ /d\vec{p}_1 d\vec{p}_2}{[d\sigma(\vec{p}_1)/d\vec{p}_1]\ [d\sigma(\vec{p}_2)/d\vec{p}_2]}$$

$$= 1 + \exp\ (-q^2R^2/2 - \omega^2\tau^2/2) \qquad (4)$$

where $\vec{q} = \vec{p}_1 - \vec{p}_2$ and $\omega = E_1 - E_2$. Thus the structure of the correlation between two identical particles with nearly identical four-momenta can be used to extract information about the space-time structure of the emitting source. Figure 10 shows recent data (74) of $\pi^-\pi^-$ correlations in 1.8 A GeV Ar + KCl collisions, in which there is a clear enhancement at small q. From these data the source radius R was determined to be 3.2 ± 0.3 fm. Recently, more data have appeared not only for two pions (75) but also for two protons (76, 77).

It is worthwhile to note that Eq. (4) holds only if the pions are emitted randomly. If pions were produced coherently (78–81), then the form of C_2 would be substantially distorted (81). For example, in the presence of a pion laser (78) the value of C_2 becomes exactly one in the entire range of $\vec{q}$. Currently, however, no definite signals for such a change in C_2 have been reported.

In order to determine ρ, it is necessary to measure m_N in coincidence with this two-particle detection. Unfortunately, no such measurements have been reported so far. However, using the estimated values of m_N an attempt to extract the value of ρ has been reported (82, 83). For Ar + KCl collisions at 1.8 GeV the density thus estimated is $\approx 2\rho_0$ when the system was probed by protons and $\approx 0.6\rho_0$ when it was probed by pions. This difference between protons and pions appears reasonable, as mentioned in Section 2.1, pions would tend to probe the

coldest and, thus, the most expanded low-density stage of the collisions. In this regard, future measurements of K^+K^+ interferometry in coincidence with m_N are particularly interesting for probing the density at the initial hot stage of the collision.

Concerning temperature, it is not a simple task to define and extract the temperature of the system, as mentioned in Sec. 2.1. However, the quantity E_0 as defined by equation (1), is closely related to the average kinetic energy carried by product particles and, thus, indicates how the nuclear matter is heated up at the stage when these product particles are emitted. We therefore may use E_0 as an effective temperature.

With these assumptions, values of density and effective temperature can be determined directly from experiments, albeit with considerable uncertainty. One can then plot these observed values in the plane of ρ and E_0. If we connect the experimental points, we can deduce how the nuclear collision evolves in time in this plane, using the different particles. From such a plot it appears (82,83) that matter at high density and temperature seems to be created in high-energy nuclear collisions. We wish to emphasize that such measurements in the future should be done under the bias of a fixed value of m_N. This is important for direct extraction of the value of ρ. It is important also for the determination of E_o, since E_0 increases as m_N increases (84,85).

3.2 Pion Multiplicity

Measurements of pion multiplicity have been performed extensively during the past few years using a streamer chamber (86-88), with which

negatively charged tracks, which are mainly from π^-, can be identified easily. Also, the average pion multiplicity, $\langle m_\pi \rangle$, has been measured with a magnetic spectrometer (11) from determination of the total integrated pion yield σ_{tot} which is related to $\langle m_\pi \rangle$ by $\sigma_{tot} = \langle m_\pi \rangle \sigma_0$ where σ_0 is the geometrical cross section. The pion multiplicity increases monotonically with beam energy as shown in Figure 11 which also illustrates various theoretical predictions.

In the past, most theoretical models have succeeded in explaining the absolute proton yield but not the pion yield. This is not surprising since the proton yield is determined mainly by the collision geometry, that is, the nucleon number associated with the participant region, whereas the pion yield directly reflects the collision dynamics. As shown in Figure 12, the thermal model (as well as the phase-space model) overpredicts the pion yield by a factor of 2-3. However, if part of the available energy remains in translational motion due to nuclear transparency or is tied up in macroscopic flow such as a radial explosion, then only the remaining energy is available for pion production, so that the pion yield is reduced (20,21,64).

Recent cascade calculations (88) also yield pion multiplicities that are higher than the experimental ones at all the beam energies, as shown in Figure 11. A reason for this discrepancy has been suggested recently (88). The basic postulate is that part of the available energy is expended as potential energy associated with the compression of the nuclear matter and this part of the energy is thus unavailable for pion production. If this potential energy is equal to E^C indicated by arrows in Figure 11, then the results of cascade

calculations would be consistent with the data. In Figure 12 this energy, E^C, is plotted as a function of the calculated density, ρ, where the latter was extracted from cascade calculations. These "data" points fall on a curve of the expected equation of state of nuclear matter with a compressibility coefficient K = 240 MeV. Therefore, it was concluded that measurements of pion multiplicity may probe the equation of state of nuclear matter. This is the first attempt at actually measuring the nuclear equation of state in high-energy collisions. It must be emphasized, though, that the method relies on the cascade code being correct in all respects other than the neglect of compressional energy. Since this assumption has been widely criticized (89-91), further investigation is called for.

3.3 Collective Flow

Let us consider an experiment of head-on collisions between U and U. Since the thickness of the U-nucleus ($\approx$15 fm) is significantly larger than the mean free path of nucleons ($\lambda \approx 2$ fm) in nuclear matter, each nucleon will experience successive NN collisions and, as a result, the local nucleon density should be increased substantially above normal during the collision. On the other hand, the NN potential contains a hard core which counteracts the creation of a local high-density region. Thus, the colliding nucleons may seek to escape from the interaction region into a region in which less nucleons exist and thus give rise to a collective flow away from the beam direction (92-100).

The first hint of such collective flow was seen in a broad sideward peak observed in 393 A·MeV Ne + U collisions (101), as shown in Figure 13. In low-multiplicity events the angular distributions are forward

peaked, whereas in high-multiplicity events the forward proton emission is highly suppressed. In addition, for low-energy protons ($E^{Lab} \simeq 12$ MeV) a broad peak is observed at $\theta = (70\text{-}90)^\circ$. This broad peak has been interpreted as due to the effect of the collective side splash of nucleons (97). It has been noted (102) that this sideward peak is predicted only with the hydrodynamical model (100) but not with the cascade (23,25,29), thermal (19), and thermal-plus-direct (49,103) models.

A second hint of a side splash is suggested by the two-proton correlations in 800 A MeV C + Pb and Ar + Pb collisions (46,104). As described in Sec. 2.2, the observed value of the in-plane to out-of-plane coincidence ratio for detection of two protons is larger than unity at $\theta > 80^\circ$ in Ar + Pb collisions. From detailed analysis of energy and angular correlations between these two protons (104) it has been found that the ratio is smaller than unity at small angles ($\theta < 70^\circ$) mainly because two high-energy protons tend to be emitted on the same side, whereas it is larger than unity at large angles ($\theta > 80^\circ$) mainly because two protons, one at high energy and the other at low energy, tend to be emitted on opposite sides. These features are what we expect from a fluid-dynamical bounce-off (97), as shown in Figure 14 since the projectile matter induces fast-fast correlations on the same side, while the projectile-target matter induces fast-slow correlations on opposite sides.

In spite of the intensive work that has gone into these two measurements, the collective effects are still weak and somewhat speculative. First, in the case of light-mass projectiles the basic assumption involved in the fluid dynamical model, i.e., $\lambda \ll R$, is not well justified even after selection of high-multiplicity events.

Second, the fluid dynamical calculations overpredict both the sidewards peak (Figure 13) and the proton-proton correlation.

In the future this topic will be revolutionized by the use of sophisticated 4π detectors such as the Plastic Ball/Wall. Early results from this detector are already showing its power for global analysis of complete events. One problem is to find a parameterization of events in which as many as a hundred particles may be detected. An attractive approach is to use the kinetic tensor, $F_{ij} = \Sigma_\nu p_i(\nu)p_j(\nu)/2m(\nu)$ which approximates the event shape by an ellipsoid whose orientation in space and aspect ratios can be calculated by diagonalizing the tensor. The orientation of the ellipse away from the beam is called the flow angle. Results obtained from Ca + Ca collisions are in reasonable agreement with cascade calculations, but preliminary data from Nb + Nb collisions (105) show clear evidence for flow angles far in excess of the predictions of these calculations as seen in Figure 15. Such behavior is predicted by fluid-dynamical calculations (106). Results from heavier systems such as Au + Au are eagerly awaited by theorists and experimentalists alike.

3.4 Cooperative Process

If nuclear matter is suddenly compressed along the beam direction as happens in a high-energy nuclear collision, the energy density may increase. This may induce meson production below the threshold energy of free NN collisions. Therefore, pion production below 290 A MeV (107-109) and K^- production below 2.5 A GeV (110) have been studied extensively.

Furthermore, pion spectra at kinetic energies beyond the free NN kinematical limit have been studied (111,112). A local high-density region may produce particle emission in the very high-p_T region (44) or in the backward direction (113-115). Such phenomena of particle emission far beyond the kinematical limits associated with free NN scattering may be called cooperative processes, since they require the cooperation of several nucleons.

Let us present an example in which cooperative particle emission is clearly observed. This is an experiment of pion production close to the absolute kinematic limit in 303 A MeV ^{3}He + ^{6}Li collisions (111,112). The data cover the region up to the absolute kinematical limit at which all the available energy is converted into a single pion while forming the ground state of the compound nucleus, ^{9}C, as shown in Figure 16. In this phenomenon, called pionic fusion, the available energy carried by individual nucleons is concentrated into a small region to create the pion. The mechanism behind this process is not yet understood and further experimental studies are desirable to see if pionic fusion can occur at different beam energies or for much heavier projectile-target combinations.

4. FRAGMENT EMISSION AT FORWARD ANGLES

In Sections 2 and 3, we focussed our attention on the fate of the participant nucleons. However, some of the earliest experiments using relativistic nuclear beams were concerned with a quite different class of events. These reactions result in the break-up of the projectile, or projectile spectator, into fragments, one or more of which are moving at close to the original beam velocity.

The inclusive yield of fragments in reactions of this type has been studied in a series of experiments using ^{4}He, ^{12}C, ^{16}O and ^{18}O beams of 1 and 2 A GeV (116–119). The momentum distributions of the fragments are found to be Gaussian in the projectile frame with widths that are small (typically 200–300 MeV/c) and that do not vary appreciably with bombarding energy, leading to the introduction of the concept of limiting fragmentation in analogy with high energy physics. It is also observed that the cross sections for production of individual isotopes can be factorized in the following way:

$$\sigma(B, F, T) = \gamma_B^F \gamma_T \qquad (5)$$

where γ_B^F depends solely on the projectile B and fragment F and γ_T is a function only of the target T.

4.1 Models of the Fragmentation Process

The observation of factorization prompted the development of a statistical model (120,121) for the reaction process in which it is assumed that the nucleus breaks up as a result of a direct reaction

between target and projectile. It was subsequently shown (122) that this model can account nicely for the variation of the measured momentum widths with the mass of the fragment if it is assumed that the fragment is formed by picking the nucleons from a Fermi gas distribution and calculating the dispersion in their momentum. This leads to an expression for the width σ of the form

$$\sigma^2 = \frac{1}{5} p^2 \times \frac{F(B-F)}{B-1} \qquad (6)$$

where B and F are, respectively, the projectile and target masses and p_F is the Fermi momentum in the nucleus and can be measured independently by, for example, electron scattering. The success of this description can be seen in Figure 17. However, it was also shown that the same dependence would be observed if the fragments were to arise from the statistical decay of an excited projectile [a model that has been applied successfully to describe the relative abundence of the different fragments (123)] and does not necessarily reflect the ground state Fermi momentum. Therefore, the measurement of momentum widths alone may be less sensitive to the reaction mechanism.

Whether the mechanism is direct break-up or excitation followed by decay, the initial interaction between projectile and target has been treated purely phenomenologically. A more complete description of the reaction is provided by the abrasion-ablation model (3,124-127). In its earliest form (3), the model assumes that the reaction can be divided into two stages, a fast one in which the participant nucleons are sheared off (abrasion), followed by statistical decay of an excited projectile remnant (ablation). This simple picture has been much refined and calculations of the abrasion stage have been made using Glauber's multiple

scattering theory (124-127) and using cascade codes (128,129). These calculations have been successful in describing ^{12}C and ^{16}O fragmentation (117) and also the fragmentation of ^{40}Ar at 213 A MeV (130).

Despite the success of these relatively simple models, it is probably premature to infer that fragmentation is well understood. This has been emphasized by several theorists who have attempted to obtain precise agreement between theory and experiment. For example, the measured momentum widths are narrower than would be expected from inelastic electron scattering by as much as 30%. At least part of this discrepancy may arise from neglect of local correlations between nucleons (131,132). A second example is the fact that factorization seems to hold much better than would be expected from the impact parameter dependence predicted by the abrasion-ablation model (133,134). It has been suggested that the process is more peripheral than can reasonably be predicted using this model (119) although it has been suggested that this may be a fortuitous consequence of measuring an inclusive cross section (135). Finally, there are obvious Coulomb effects that become important as the bombarding energy is reduced below 100 A MeV (136-138), indicating that limiting fragmentation is only valid above this energy.

Small but significant deviations of this kind have led to the introduction of a new, peripheral, model (139) for fragmentation that includes effects of absorption of the fragments by the target. In this model, the separation energy of the fragment becomes the most important physical parameter in determining the momentum width. This model has succeeded in describing simultaneously the detailed structure of the momentum widths, in particular the variation in width of different

fragments of the same mass, the relative isotopic yields and the Coulomb effects. In summary there is a clear need for further experimental information to elucidate the reaction mechanism of projectile fragmentation. The more detailed information that will come from studies using multi-particle spectrometers will obviously be important, but further inclusive experiments using heavy projectiles should not be neglected.

4.2 Electromagnetic Effects

So far, we have assumed that the interaction between projectile and target is a purely nuclear one. This is inadequate in some cases, in particular for those reaction channels where the corresponding photo-nuclear cross section is large and when the charge of the target is high. The cross sections for this process can be calculated using the Weizsäcker-Williams theory (140) to obtain the virtual photon spectrum and coupling this to the appropriate photo-disintegration cross section. Unfortunately, this process is essentially indistinguishable from a nuclear process leading to the same final state. This problem can, however, be overcome using the factorization property of fragmentation reactions if the yield is measured from a series of different targets. In general, the electromagnetic process will only contribute strongly to a few channels, in particular those leading to single particle removal. One can therefore obtain the target factors, γ_T, using channels for which electromagnetic dissociation is negligible and thence estimate the nuclear background for the channels of interest and subtract it from the experimentally observed cross section. This procedure has been used with

considerable success in studying the fragmentation of ^{16}O, ^{18}O and ^{56}Fe (141-143) and is illustrated in Figure 18. The absolute cross sections are in good agreement with the Weizsäcker-Williams predictions and with those of more sophisticated models (144) for the virtual photon spectrum.

Another example of electromagnetic effects is seen in pion production at forward angles. Figure 19 shows the π^- yield for ^{20}Ne and ^{40}Ar induced reactions (145,107). The π^- yield has a strong peak (and the corresponding π^+ yield has a dip) at the projectile velocity. This feature is understood as resulting from the Coulomb forces of other projectile fragments on the light-mass pion (146).

4.3 Applications of Fragmentation Reactions

The results of fragmentation reactions are having important additional consequences. The most exciting example is the very considerable potential for fragmentation reactions to increase our knowledge of nuclear structure. We have already noted the wide range of nuclear fragments that are produced in these reactions. Indeed almost any combination of the neutrons and protons inside a projectile will be emitted at some level. The important question is whether nuclei far from the valley of stability such as ^{8}He or ^{34}Mg will be produced sufficiently often to be measurable in the laboratory This question has been answered empirically by experiments using high energy nuclear beams that have discovered a variety of light neutron-rich isotopes (147-149). It is important to note that whereas the cross sections are comparable to those of other techniques, the beam intensities are

typically five orders of magnitude less, demonstrating the very high efficiency of the fragmentation technique. This comes from the excellent collimation of the fragments in the beam direction and the ability to use thick targets.

The persistence of velocity also enables the fragments to be used in secondary beam experiments with very high efficiency. Many conventional aspects of nuclear structure study can then be extended to unstable nuclei with half lives as short as a few milliseconds and that are innaccessible to conventional techniques. Some half-life measurements have already been made (150) and several novel experiments are planned including studies of mirror magnetic moments, electromagnetic dissociation and reaction cross sections.

A further example of the application of our knowledge of fragmentation reactions is in cosmic ray physics. The species distribution of cosmic rays detected on earth or by satellite may be substantially different from that at their source because of reactions in the interstellar medium. Measured fragmentation cross sections can be used to correct the observed yields.

A final example is in the use of heavy ion beams for medical purposes such as tomography and radiotherapy. In the latter case, one is taking advantage of the fact that the ionization by a heavy ion is greatest at the end of its range which can be used to reduce the radiation damage to healthy tissue. However, the incident beam can break up before coming to rest and a precise knowledge of fragmentation systematics is needed to calculate the dose distribution correctly.

5. SUMMARY AND FUTURE PERSPECTIVES

As stated in the Introduction, the field of high-energy nuclear collisions is in a state of rapid development. During the past 5-10 years a large body of experimental data has been accumulated. In particular, single-particle and two-particle inclusive distributions have been measured for a variety of projectile and target combinations at beam energies from 200 A MeV to 2 A GeV. From these studies it has become clear that a high-energy nuclear collision is a non-equilibrium many-body process which includes not only the primary NN collisions but also collisions between the product particles, such as pions, and the surrounding nucleons. With the exception of a few experimental variables, such as the d/p ratio and pion multiplicity, it seems that the dominant reaction mechanism can be described quite well using multiple-collision theories with very reasonable theoretical assumptions.

Currently, the following three subjects are being studied intensively. The first one concerns the creation of hot, dense nuclear matter and its properties. As discussed in Sec. 3.1, it is likely that such nuclear matter is created in high-energy nuclear collisions. We have seen that attempts to study its properties matter have started from the analysis of d/p ratios (Sec. 2.3) or pion multiplicity (Sec. 3.2) although the conclusions are still controversial and the subject of lively debate.

The second subject is the search for new dynamic modes that are produced during the course of a nuclear collision. This has been discussed in Secs. 3.3 and 3.4. Some preliminary results are already available that indicate the presence of nucleonic flow and this is one

field where one really can expect to make significant progress in the near future. Sophisticated detectors designed specifically to measure multiparticle final states such as the Plastic Ball/Wall and HISS (151), are just coming into use as are the heavy beams needed for these studies. Particle emission beyond the free NN kinematical limit is another indication of cooperative behavior between nucleons. We have noted the phenomenon of pionic fusion for light-mass collisions, in which the total available kinetic energy in the c.m. frame is converted to emission of a single pion. We have also mentioned subthreshold pion emission and high-p_T particle emission. From these studies it is clear that processes certainly exist that cannot be explained by the superposition of incoherent NN collisions.

The third subject is related to physics of projectile fragments, as discussed in Sec. 4. Although there are some unknowns in the production mechanism of these fragments, physics of projectile fragments is a unique feature of high-energy nuclear collisions. Strong Coulomb interactions induce a large photo-nuclear cross section as well as a large π^-/π^+ ratio. A fascinating aspect of projectile fragments is the production of unstable nuclei far from the stability line and their application to nuclear physics. Since these nuclei are emitted in a very restricted kinematic domain they can be used as high-quality secondary beams as well.

One of the ultimate goals in the research of high energy nuclear collisions is to create and study matter which is different from the normal nuclear matter seen in stable nuclei. High energy nuclear collisions may transform the nucleons into other baryons, such as Δ, N*, Λ, and also create mesons, such as π,ρ, K, so we may expect the production

of matter containing these particles. Their quantum numbers differ from those of the nucleons and they may be considered as impurities in the nuclear matter. For example, the behavior of a ρ meson imbedded in nuclear matter is of interest for the understanding of nuclear forces. Another example is the formation of a projectile fragment in which a produced particle is trapped. Such hypernuclei have been studied rather extensively with mesonic probes, but nuclear collisions offer the possibility of forming hypernuclei with multiple strangeness. If the impurity level is high enough, then the matter may change its character. For example, at 700 A MeV 50 of the NN collisions create Δ's, which might then result in an interesting new form of baryonic matter containing mostly Δ particles (152).

Recently there has been wide discussion of a more dramatic change in the properties of nuclear matter that may take place in a high energy nuclear collision. It has been suggested that a phase transition from hadronic matter into a quark-gluon plasma may occur at high density and pressure (153,154). This transition would involve simultaneously the break-down of quark confinement and the formation of a new type of many-body system and is of fundamental importance to both nuclear and particle physics. At the present stage, the exact form of the transition and the way in which it would become manifest are unclear. However, there does seem to be a consensus that the presently available energies are too low and new experimental facilities are currently being planned. We feel confident that the experience already gained from the studies described in this review will prove invaluable for this new venture.

ACKNOWLEDGEMENT

We are very grateful to all of our colleagues who have assisted us with material and advice during our preparation of this review.

This work is supported by the Director, Office of Energy Research Division of Nuclear Physics of the Office of High Energy and Nuclear Physics of the U.S. Department of Energy under Contract No. DE-AC03-76SF00098.

References

1. Heckman, H., 1983, private communication
2. Eisenberg, Y., 1954. Phys. Rev. 96: 1378
3. Bowman, J. D., Swiateki, W. J., Tsang, C. F., 1973, Lawrence Berkeley Laboratory report No. LBL-2908
4. Nagamiya, S. 1980. Nucl. Phys. A355: 517c
5. Manko, V. I., Nagamiya, S. 1982. Nucl. Phys. A384: 475
6. Weise, R., Brown, G. E. 1976. Phys. Reports 27C: 1
7. Migdal, A. B., 1978. Rev. Mod. Phys. 50: 107
8. Lee, T. D., Wick, G. C., 1974. Phys. Rev. D9: 2291
9. Lee, T. D., 1976. Rev. Mod. Phys. 47: 267
10. Jacob, M., Tran Thanh Van, J., 1982. Phys. Reports 88C: 321
11. Nagamiya, S., Lemaire, M.-C., Moeller, E., Schnetzer, S., Shapiro, G., et al. 1981. Phys. Rev. C24: 971
12. Randrup, J., 1978. Phys. Lett. 76B: 547
13. Sobel, M., Siemens, P. J., Bondorf, J. P., Bethe, H. A. 1975. Nucl. Phys. A251: 502
14. Westfall, G. D., Gosset, J., Johansen, P. J., Poskanzer, A. M., Meyer, W. G., et al., 1976. Phys. Rev. Lett. 37: 1202
15. Kapusta, J. I. 1977. Phys. Rev. C16: 1493
16. Mekjian, A. Z., 1978. Phys. Rev. C17: 1051
17. Das Gupta, S., Mekjian, A. Z. 1981. Phys. Reports 72C: 131
18. Myers, W. D. 1978. Nucl. Phys. A296: 177
19. Gosset, J., Kapusta, J. I., Westfall, G. D. 1978. Phys. Rev. C18: 844
20. Das Gupta, S., 1978. Phys. Rev. Lett. 41: 1450
21. Siemens, P. J., Rasmussen, J. O. 1979. Phys. Rev. Lett. 42: 844
22. Gudima, K. K., Toneev, V. D., 1978. Yad. Fiz. 27:658 [Sov. J. Nucl. Phys. 27:351]
23. Stevenson, J. D. 1978. Phys. Rev. Lett. 41: 1702
24. Gudima, K. K., Iwe, H., Toneev, V. D., 1979. J. Phys. G5:229
25. Yariv, Y., Fraenkel, Z. 1979. Phys. Rev. C20: 2227
26. Cugnon, J. 1980. Phys. Rev. C22: 1885
27. Cugnon, J., Mizutani, T., Vandermeulen, J. 1981. Nucl. Phys. A352: 505

28. Cugnon, J., Kinet, J., Vandermeulen, J. 1982. Nucl. Phys. A379: 553
29. Yariv, Y., Fraenkel, Z. 1981. Phys. Rev. C24: 488
30. Hüfner, J., Knoll, J., 1977. Nucl. Phys. A290: 460
31. Hüfner, J. 1978. Proc. 4th High-Energy Heavy Ion Summer Study, LBL-7766, Conf-780766: 135
32. Knoll, J. 1979. Phys. Rev. C20: 773
33. Bohrmann, S., Knoll, J. 1981. Nucl. Phys. A356: 498
34. Schnetzer, S., Lemaire, M.-C., Lombard, R., Moeller, E., Nagamiya, S., et al., Phys. Rev. Lett. 49: 989
35. Randrup, J., Ko, C. M. 1980. Nucl. Phys. A343: 519
36. Asai, F. 1981. Nucl. Phys. A356: 519
37. Nagamiya, S. 1982. Phys. Rev. Lett. 49: 1383
38. Randrup, J. 1981. Phys. lett. 99B: 9
39. Zwermann, W., Schürmann, B., Dietrich, K., Martschew, E. 1983. Phys. Lett. B (in press)
40. Cugnon, J., Lombard, R. 1983. Phys. Lett. B (in press)
41. Asai, F., Sato, H., Sano, M., 1981. Phys. Lett. 98B: 19
42. Ko, C. M. 1981. Phys. Rev. C23: 2760
43. Halemane, T. R., Mekjian, A. Z. 1982. Phys. Rev. C25: 2398
44. Hamagaki, H., Bai, X. X., Hashimoto, O., Kadota, S., Kimura, K., et al., 1984. LBL-17276 preprint.
45. Nagamiya, S., Anderson, L., Brückner, W., Chamberlain, O., Lemaire, M.-C., et al., 1978. Phys. Lett. 81B: 147
46. Tanihata, I., Lemaire, M.-C., Nagamiya, S., Schnetzer, S. 1980. Phys. Lett. 97B: 363
47. Tanihata, I., Nagamiya, S., Schnetzer, S., Steiner, H. 1981. Phys. Lett. 100B: 121
48. Pirner, H. J., Schürmann, B. 1979. Nucl. Phys. A316: 461
49. Chemtob, M., Schürmann, B. 1980. Nuc. Phys. A336: 508
50. Gutbrod, H. H., Sandoval, A., Johansen, P. J., Poskanzer, A. M., Gosset, J., et al., 1976. Phys. Rev. Lett. 37: 667
51. Lemaire, M.-C., Nagamiya, S., Schnetzer, S., Steiner, H., Tanihata, I. 1979. Phys. Lett. 85B: 38
52. Knoll, J., Randrup, J., 1981. Phys. Lett. 103B: 264
53. Butler, S. F., Pearson, C. A. 1963. Phys. Rev. 129: 836

54. Schwarzschild, A., Zupančič, C. 1963. Phys. Rev. 129: 854
55. Sandoval, A., Gutbrod, H. H., Meyer, W. G., Stock, R., Lukner, Ch., et al., 1980. Phys. Rev. C21:1321
56. Bond, R., Johansen, P. J., Koonin, S. E., Garpman, S. 1977. Phys. Lett. 71B: 43
57. Jennings, B. K., Das Gupta, S., Mobed, N., 1981. Phys. Rev. 25:278
58. Bertsch, G. F. 1983. Nucl. Phys. A400: 221c
59. Gutbrod, H. H., Löhner, H., Poskanzer, A. M., Penner, T., Riedesel, H., et al., 1983. Phys. Lett. 127B: 317
60. Gutbrod, H. H., Löhner, H., Poskanzer, A. M., Penner, T., Riedesel, H., et al., 1983. Nucl. Phys. A400: 343c
61. Sato, H., Yazaki, K. 1981. Phys. Lett. 98B: 153
62. Siemens, P. J., Kapusta, J. I. 1979. Phys. Rev. Lett 43: 1486, 1690(E)
63. Bertsch, G. F., Cugnon, J. 1981. Phys. Rev. C24: 2514
64. Kapusta, J. I., Strottman, D. 1981. Phys. Rev. C23: 971, 1282
65. Csernai, L. P., Barz, H. W. 1980. Z. Physik A296: 173
66. Das Gupta, S., Jennings, B. K., Kapusta, J. I. 1982. Phys. Rev. C26: 274
67. Fai, G., Randrup, J., 1981. Nucl. Phys. A381: 557
68. Hanbury-Brown, R., Twiss, R. Q. 1956. Nature 178: 1046
69. Goldhaber, G., Goldhaber, S., Lee, W., Pais, A. 1960. Phys. Rev. 120: 300
70. Cocconi, G. 1974. Phys. Lett. 49B: 459
71. Kopylov, G. I. 1974. Phys. Lett. 50B: 572
72. Koonin, S. E., 1977. Phys. Lett. 70B: 43
73. Yano, F. B., Koonin, S. E. 1978. Phys. Lett. 78B: 556
74. Zajc, W. A., Bistirlich, J. A., Bossingham, R. R., Bowman, H. R., Clawson, C. W., et al., 1981. Proc. 5th High-Energy Summer Study, Berkeley, LBL-12652: 350
75. Beavis, D., Fung, S. Y., Gorn, W., Huie, A., Keane, D., et al., 1983. Phys. Rev. C27: 910
76. Zarbakhsh, Z., Sagle, A. L., Brochard, F., Mulera, T. A., Perez-Mendez, V., et al., 1981. Phys. Rev. Lett. 36: 1268

77. Wieman, H., Gutbrod, H. H., Gustafsson, H. A., Kolb, B., Löhner, H., et al., 1983. Proc. of the Sith High Energy Heavy Ion Study, Berkeley, LBL-16281:325
78. Chapline, C. F., Johnson, H. H., Teller, E., Weiss, M. S. 1973. Phys. Rev. D8: 4302
79. Deutchmann, P. A., Townsend, L. W. 1980. Phys. Rev. Lett. 45: 1622
80. Gyulassy, M., Kauffmann, S. K., Wilson, L. W. 1979. Phys. Rev. C20: 2267
81. Gyulassy, M. 1982. Phys. Rev. Lett. 48: 454
82. Nagamiya, S. 1983. Nucl. Phys. A400: 399c
83. Nagamiya, S. 1984. Nucl. Phys. (in press)
84. Nagamiya, S., Lemaire, M.-C., Schnetzer, S., Steiner, H., Tanihata, I., 1980. Phys. Rev. lett. 45: 602
85. Gutbrod, H. H., Gustafsson, H. A., Kolb, B., Löhner, H., Ludewigt, B., et al., 1982. Proc. 6th Balaton Topical Conf. on High-Energy Nuclear Phys.: 269
86. Fung, S. Y., Gorn, W., Kiernan, G. P., Liu, F. F., Lu, J. J., et al., 1978. Phys. Rev. Lett. 40: 292
87. Sandoval, A., Stock, R., Stelzer, H. E., Renfordt, R. E., Harris, J. W., et al., 1980. Phys. Rev. Lett. 45: 874
88. Stock, R., Bock, R., Brockman, R., Harris, J. W., Sandoval, A., et al., 1982. Phys. Rev. Lett. 49: 1236
89. Malfliet, R., Schürmann, B. 1983. Phys. Rev. C28: 1136
90. Bertsch, G. F., Kruse, H., Das Gupta, S. 1983. preprint.
91. Cahay, M., Cugnon, J., Vanbdermuelen, J., 1983, Nucl. Phys. A411:524
92. Scheid, W., Muller, H. Greiner, W. 1974. Phys. Rev. Lett. 32: 741
93. Amsden, A. A., Bertsch, G. F., Harlow, F. H., Nix, J. R. 1975. Phys. Rev. Lett. 35: 905
94. Kitazoe, Y. Matsuoka, K., Sano, M. 1976., Prog. Theor. Phys. 56: 860
95. Bondorf, J. P. Garpman, S. I. A., Zimanyi, J. 1978. Nucl. Phys. A296: 320
96. Nix, J. R. Prog. Part. Nucl. Phys. 2: 237
97. Stöcker, H., Maruhn, J. A., Greiner, W. 1980. Phys. Rev. Lett. 44: 725
98. Tang, H. H. K., Wong, C. Y. 1980. Phys. Rev. C21: 1846

99. Stöcker, H., Hofmann, J., Maruhn, J. A., Greiner, W. 1980. Prog. Part. Nucl. Phys. 4: 133
100. Nix, J. R., Strottman, D. 1981. Phys. Rev. C23: 2548
101. Stock, R., Gutbrod, H. H., Meyer, W. G., Poskanzer, A. M., Sandoval, A., et al., 1980. Phys. Rev. Lett. 44:1243
102. Stöcker, H., Riedel, C., Yariv, Y., Csernai, L. P., Buchwald, G., et al., 1981. Phys. Rev. Lett. 47: 1807
103. Schürmann, B., Chemtob, M. 1980. Z. Physik A294: 371
104. Csernai, L. P., Greiner, W., Stöcker, H., Tanihata, I., Nagamiya, S., et al., 1982. Phys. Rev. C25: 2482
105. Ritter, H. G., Gustafsson, H. A., Gutbrod, H. H., Kolb, B., Löhner, H., et al., 1983. Proceedings on 6th High-Energy Heavy-Ion Study and 2nd Workshop on Anomalons, LBL-16281:191
106. Csernai, L. P., Stöcker, H., Subramanian, P. R., Graebner, G., Rosenhauer, A., et al., 1983. Phys. Rev. C28: 2001
107. Benenson, W., Bertsch, G. F., Crawley, G. M., Kashy, E., Nolen, J. A., et al., 1979. Phys. Rev. Lett. 43: 683, 44: 54(E)
108. Johansson, T., Gustafsson, H. A., Jacobsson, B., Kristiansson, P., Norén, B., et al. 1982. Phys. Rev. Lett. 48: 732
109. Nagamiya, S., Hamagaki, H., Hecking, P., Lombard, R., Miake, Y., et al.,. 1982. Phys. Rev. lett. 48: 1708
110. Shor, A., Ganezer, K., Abachi, S., Carroll, J., Geaga, J., et al., 1982. Phys. Rev. Lett. 48: 1597
111. Aslanides, E., Fassnacht, P., Hibou, F., Chiavassa, E., Dellacasa, G., et al., 1979. Phys. Rev. Lett. 43: 1466; 45:1738(E)
112. Aslanides, E., et al. 1984, private communication
113. Baldin, A. M. 1975. AIP Conference Proceedings 26: 621
114. Baldin, A. M., Guiordenescu, M., Zubarev, V. N., Moroz, N. S., Povtoreiko, A. A., et al., 1975. Yad. Fiz 20: 1201 [Sov. J. Nucl. Phys. 20: 629]
115. Schroeder, L. S., Chessin, S. A., Geaga, J. V., Grossiord, J. Y., Harris, J. W., et al., 1979. Phys. Rev. Lett. 43: 1787
116. Anderson, L., Brükner, W., Moeller, E., Nagamiya, S., Nissen-Meyer, S., et al., 1983. Phys. Rev. C28: 1224

117. Heckman, H. H., Greiner, D. E., Lindstrom, P. J., Bieser, F. S., 1972. Phys. Rev. Lett. 27: 926
118. Lindstrom, P. J., Greiner, D. E., Heckman, H. H., Cork, B., Bieser, F. S., 1975, Lawrence Berkeley Laboratory report No. LBL-3650
119. Olson, D. L., Berman, B. L., Greiner, D. E., Heckman, H. H., Lindstrom, P. J., et al., 1983. Phys. Rev. C28: 1602
120. Feshbach, H., Huang, K., 1973. Phys. Lett. 47B: 300
121. Bhaduri, K., 1974. Phys. Lett. 50B: 311
122. Goldhaber, A. S., 1974. Phys. Lett. 53B: 306
123. Lukyanov, V. K., Titov, A. L., 1975. Phys. Lett. 57B: 10
124. Hüfner, J., Schaffer, K., Schurmänn, B., 1975. Phys. Rev. C12: 1888
125. Abul-Magd, A., Hüfner, J., Schürmann, B., 1976. Phys. Lett. 60B: 327
126. Abul-Magd, A., Hüfner, J., 1976. Z. Phys. A277: 379
127. Hüfner, J., Sander, C., Wolschin, G., 1978. Phys. Lett. 73B: 2891
128. Morrissey, D. J., Oliveira, L. F., Rasmussen, J. O., Seaborg, G. T., Yariv, Y., et al., 1979. Phys. Rev. Lett. 43: 1139
129. De Oliveira, L. F., 1978, PhD. Thesis, U.C. Berkeley, 1978, Lawrence Berkeley Laboratory Report LBL-8561
130. Viyogi, Y. P., Symons, T. J. M., Doll, P., Greiner, D. E., Heckman, H. H., et al., 1979. Phys. Rev. Lett. 42:33
131. Bertsch, G., 1981. Phys. Rev. Lett. 46: 472
132. Murphy, M. J., 1984. Phys. Rev. Lett. in press
133. Bleszynski, M., Sander, C., 1979. Nuc. Phys. A326: 525
134. Cugnon, J., Sartor, R., 1980. Phys. Rev. C21: 2342
135. Stevenson, J. D., Martinis, J., Price, P. B., 1981. Phys. Rev. Lett. 47: 990
136. Van Bibber, K., Hendrie, D. L., Scott, D. K., Wieman, H. H., Schroeder, L. S., et al., 1979. Phys. Rev. Lett. 43: 840
137. Mougey, J., Ost, R., Buenerd, M., Cole, A. J., Guet, C., et al., 1981. Phys. Lett. 105B: 25
138. Wong, C. Y., Van Bibber, K., 1982. Phys. Rev. C25: 1460
139. Friedman, W., 1983. Phys. Rev. C27:569
140. Williams, E. J., 1933, Prog. Roy. Soc. A139: 163
141. Heckman, H. H., Lindstrom, P. J., 1976. Phys. Rev. Lett. 37: 56

142. Olson, D. L., Berman, B. L., Greiner, D. E., Heckman, H. H., Lindstrom, P. J., et al., 1981. Phys. Rev. C24: 1529
143. Westfall, G. D., Wilson, L. W., Lindstrom, P. J., Crawford, H. J., Greiner, D. E., 1979. Phys. Rev. C19: 1309
144. Jäckle, R. R., Pilkuhn, H., 1975. Nuc. Phys. A247: 521
145. Sullivan, J. P., Bistirlich, J. A., Bowman, H. R., Bossingham, R., Buttke, T., et al., 1982. Phys. Rev. C25: 1499
146. Radi, H. M. A., Rasmussen, J. O., Sullivan, J. P., Fraenkel, K. K., Hashimoto, O., 1982. Phys. Rev. C25, 1518
147. Symons, T. J. M., Viyogi, Y. P., Westfall, G. D., Doll, P., Greiner, D. E., et al., 1979. Phys. Rev. Lett. 42: 40
148. Westfall, G. D., Symons, T. J. M., Greiner, D. E., Heckman, H. H., Lindstrom, P. J., et al., 1979. Phys. Rev. Lett. 43: 1859
149. Stevenson, J. D., Price, P. B., 1981. Phys. Rev. C24: 2101
150. Murphy, M. J., Symons, T. J. M., Westfall, G. D., Crawford, H. J., 1982. Phys. Rev. Lett. 49: 455
151. Greiner, D. E., 1983. Nucl. Phys. A400: 325c
152. Kondratyuk, L. A., Shapiro, I. S., 1970. Yad. Fix. 12: 401 [Sov. J. Nucl. Phys. 12: 220]
153. Jacob, M., Satz, H., ed., 1982. Quark Matter Formation and Heavy Ion Collisions, World Scientific, Singapore
154. Proceedings of Quark Matter '83, Nucl. Phys. (in press)
155. Stöcker, H., 1981. Lawrence Berkeley Laboratory Report. LBL-12302
156. Gyulassy, M., Fraenkel, K. A., Stöcker, H., 1982. Phys. Lett. 110 B: 185

Figure Captions

Figure 1 Recording of a collision between a 1 A GeV U projectile nucleus with a target nucleus in an emulsion (1).

Figure 2 Participant-spectator separation expected in high-energy nucleus-nucleus collisions.

Figure 3 Theoretical expectations of new phases for hot and dense nuclear matter.

Figure 4 Left: Proton energy spectra at c.m. 90° in collisions of 800 A MeV C + C, Ne + NaF, and Ar + KCl (11). Dashed curve indicates the calculated result from the single NN collision model with a Gaussian type Fermi motion included (12).

Right: Angular distribution of protons in the c.m. frame in 800 A MeV Ar + KCl collisions for three different proton energies (11).

Figure 5 Energy spectra of K^+ in the c.m. frame in 2.1 A GeV Ne + NaF collisions. The figure is made from the data reported in ref. (34).

Figure 6 Recent data of proton energy spectra at c.m. 90° in 800 A MeV C + C collisions (44).

Figure 7 Energy-integrated angular distributions of the in-plane to out-of-plane ratio, C, for two protons emitted in 800 A MeV C + C and Ar + Pb collisions. Figure made from the data reported in refs (45,46,104).

Figure 8 Deuteron and triton spectra in 800 A MeV C + C collisions, as compared with the second and third power, respectively, of the observed proton spectra (11).

Figure 9 Ratios of d_{Like} plotted as a function of the value of p_{Like}. Data were taken by the plastic Ball-Wall (58,59). Here, d_{Like} is defined $N_d + 1.5\ (N_t + N_{^3He}) + 3\ N_\alpha$, whereas p_{Like} is defined $N_p + N_d + N_t + 2\ (N_{^3He} + N_\alpha)$. Taken from ref. (85).

Figure 10 Two-pion interferometry observed in 1.8 A GeV Ar + KCl collisions. Data are taken from ref. (74).

Figure 11 Observed pion multiplicities as compared with the results of thermal (FB), hydrodynamical (with various viscosities), and cascade calculations for central collisions of Ar + KCl. Figures taken from refs. (155) and (88).

Figure 12 Values of E^C, defined in Figure 11, plotted as a function of the calculated mean baryon density. Dashed curves are based on conventional equations of state. Figure taken from ref. (88).

Figure 13 Proton angular distributions for high-multiplicity (upper) and low-multiplicity events in 393 A MeV Ne + U collisions (101).

Figure 14 Hydrodynamical side splash (upper) and bounce off (lower) predicted in ref. (97).

Figure 15 Flow angle distributions for different multiplicity bins in 400 A MeV Nb + Nb collisions (105). Also shown are the predictions of cascade calculations (156).

Figure 16 Pion momentum spectrum measured at 0° at around the kinematical limit of pion emission in 303 A MeV ^{3}He + ^{6}Li collisions. Data are provided by Aslanides et al. (112).

Figure 17 Momentum widths of the isotopes produced in fragmentation of ^{16}O at 2.1 A GeV (117).

Figure 18 Relative cross sections for isotope production by fragmentation of ^{18}O at 1.8 A GeV showing the enhancement due to electromagnetic dissociation in one and two nucleon removal channels (142).

Figure 19 π^- spectrum at 0° for 280 A GeV ^{20}Ne + ^{12}C (145,146). The theoretical curves (146) are shown for three different choices of fragmentation velocity and dispersion parameter σ_0.

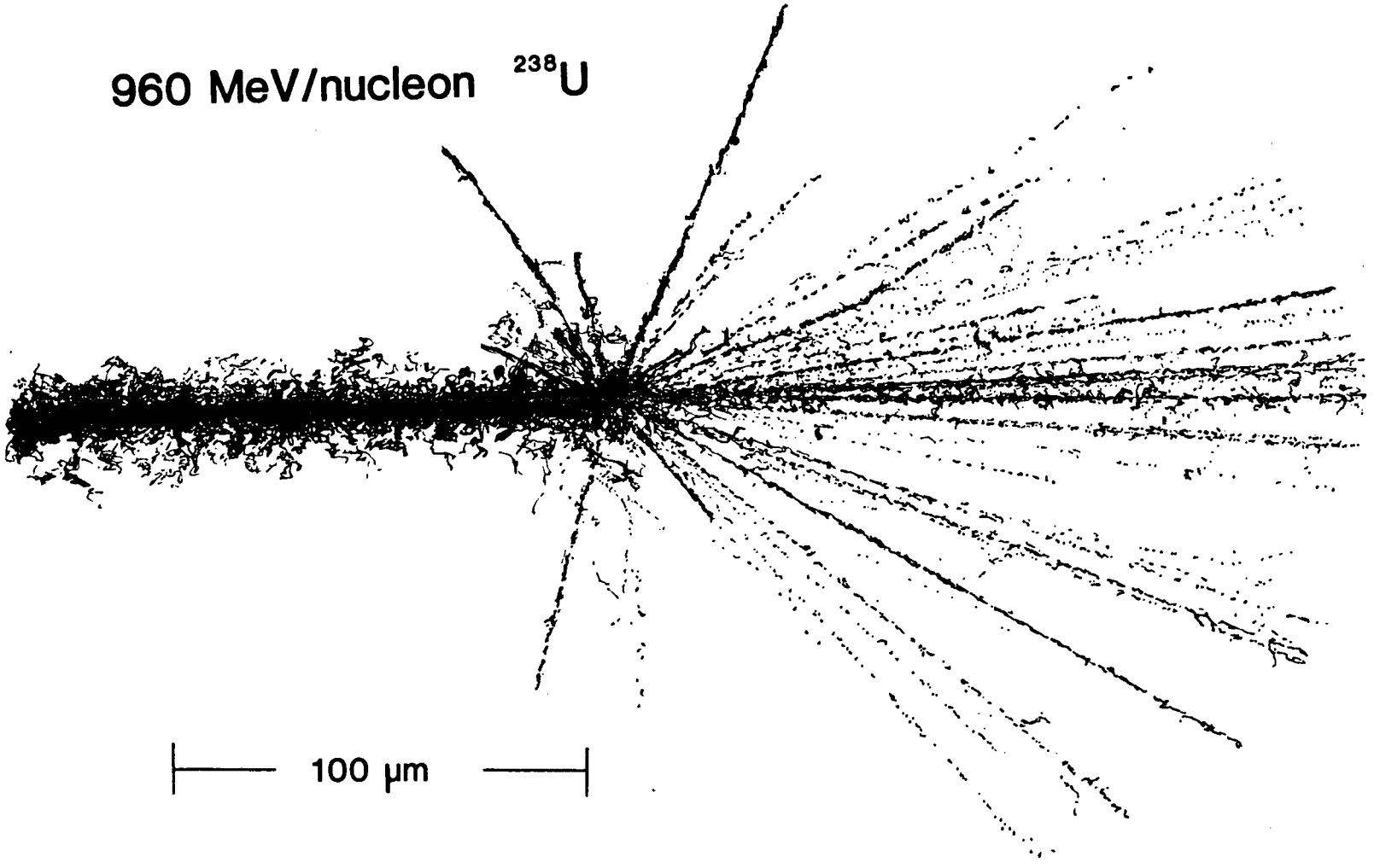

XBL 829-11834

Fig. 1

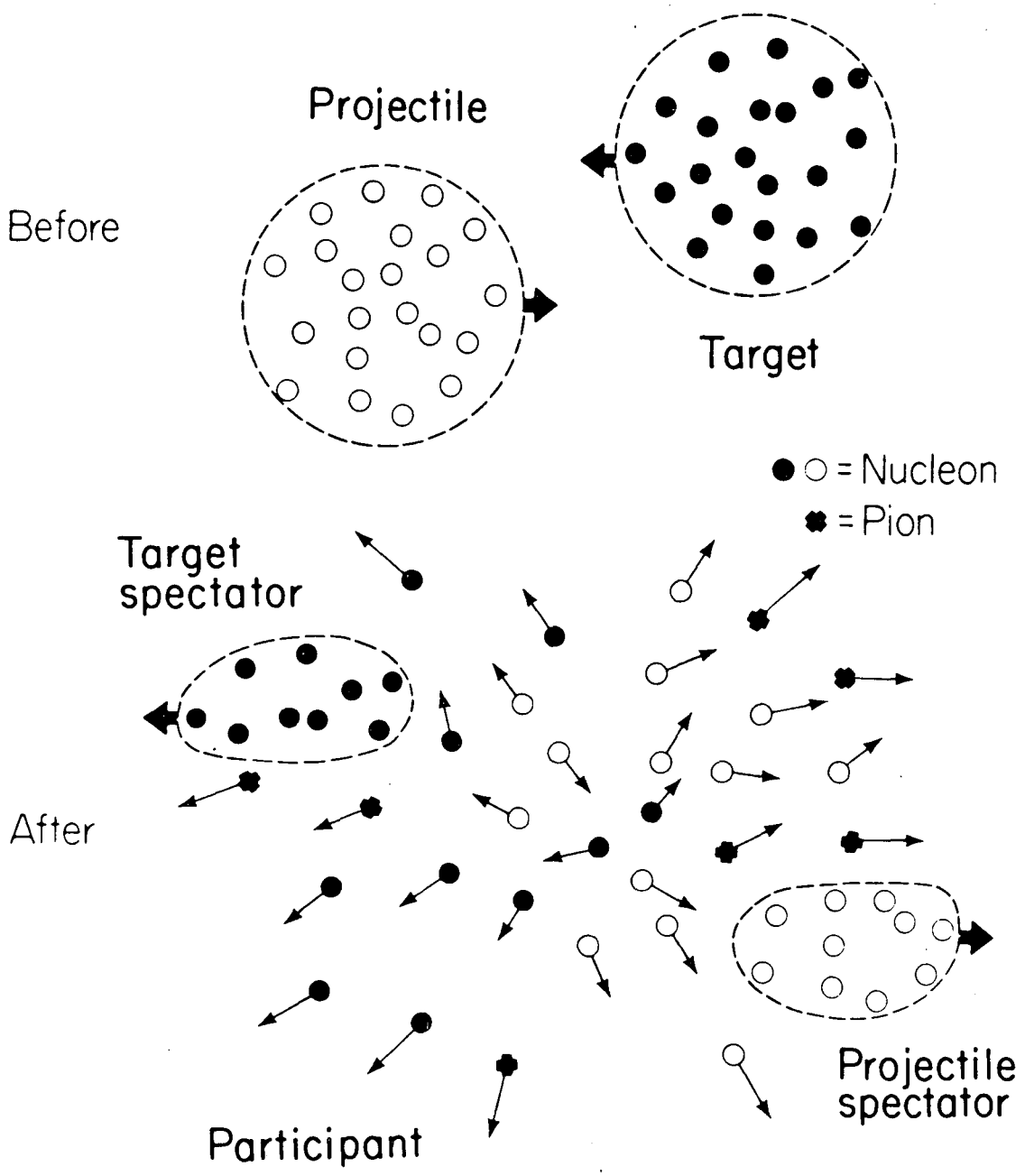
Projectile
Before
Target
● ○ = Nucleon
✱ = Pion
Target
spectator
After
Participant
Projectile
spectator
XBL 8012-2526A

Fig. 2

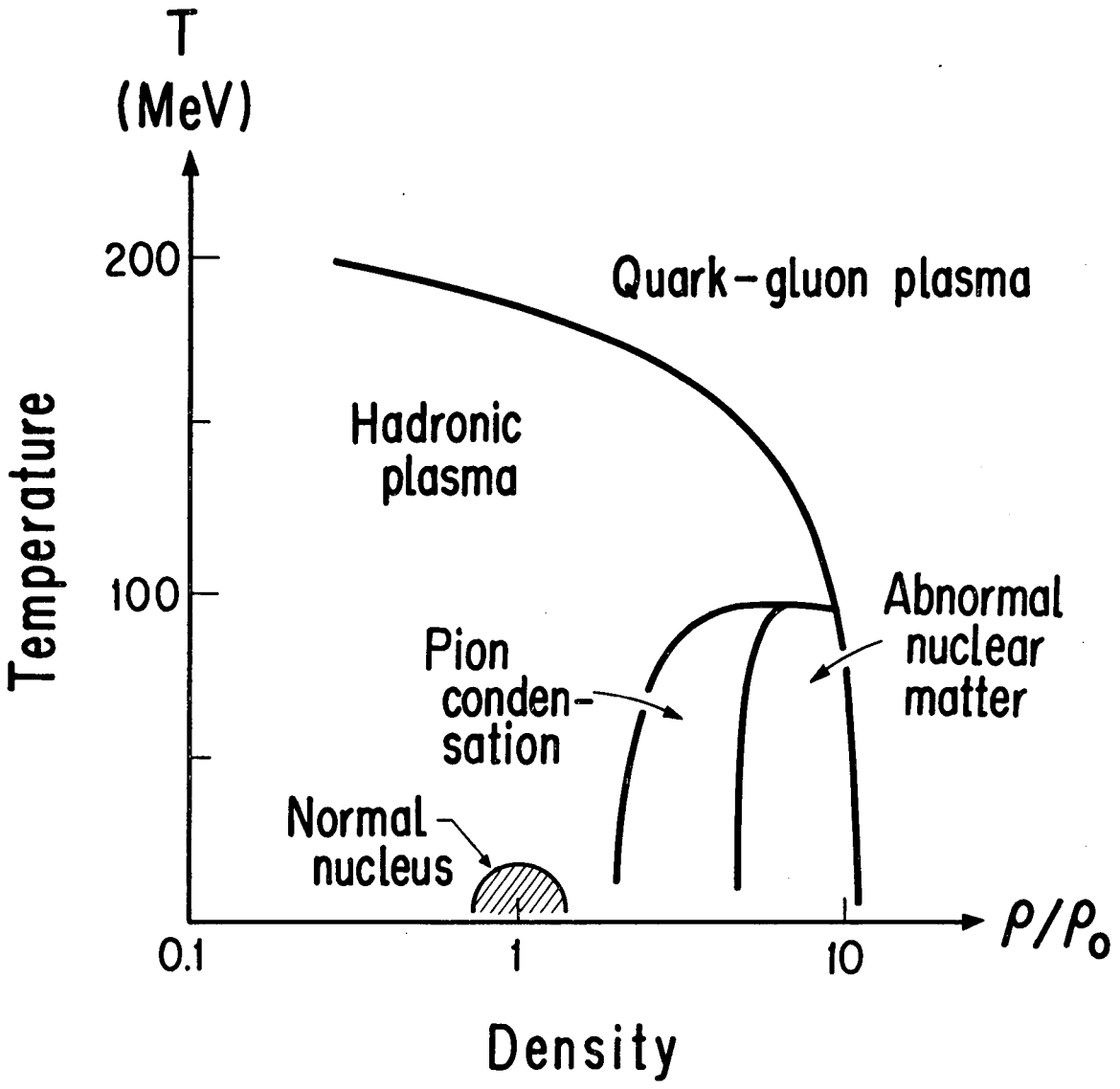

XBL 841-281

Fig. 3

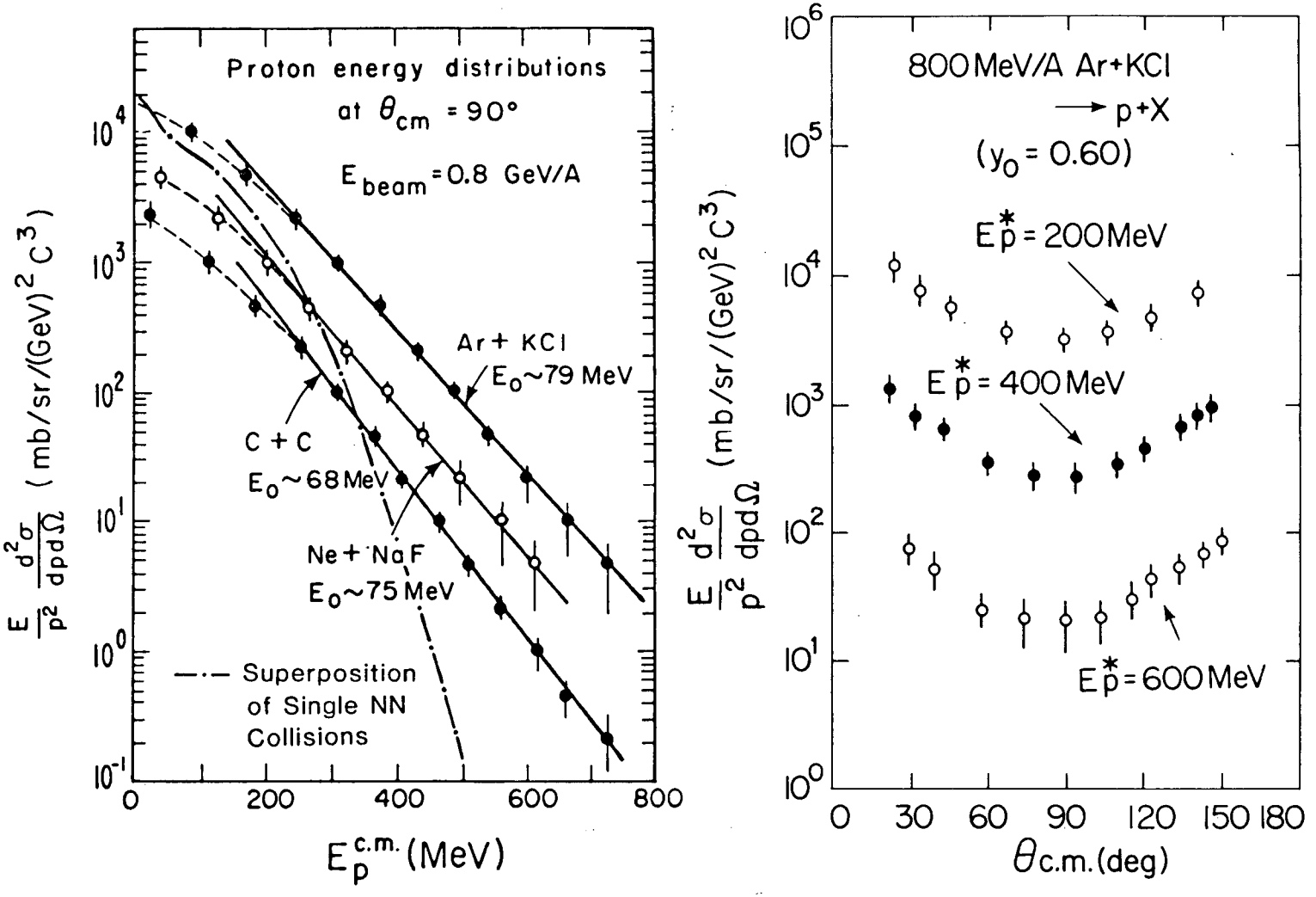

XBL 797-2085B

Fig. 4

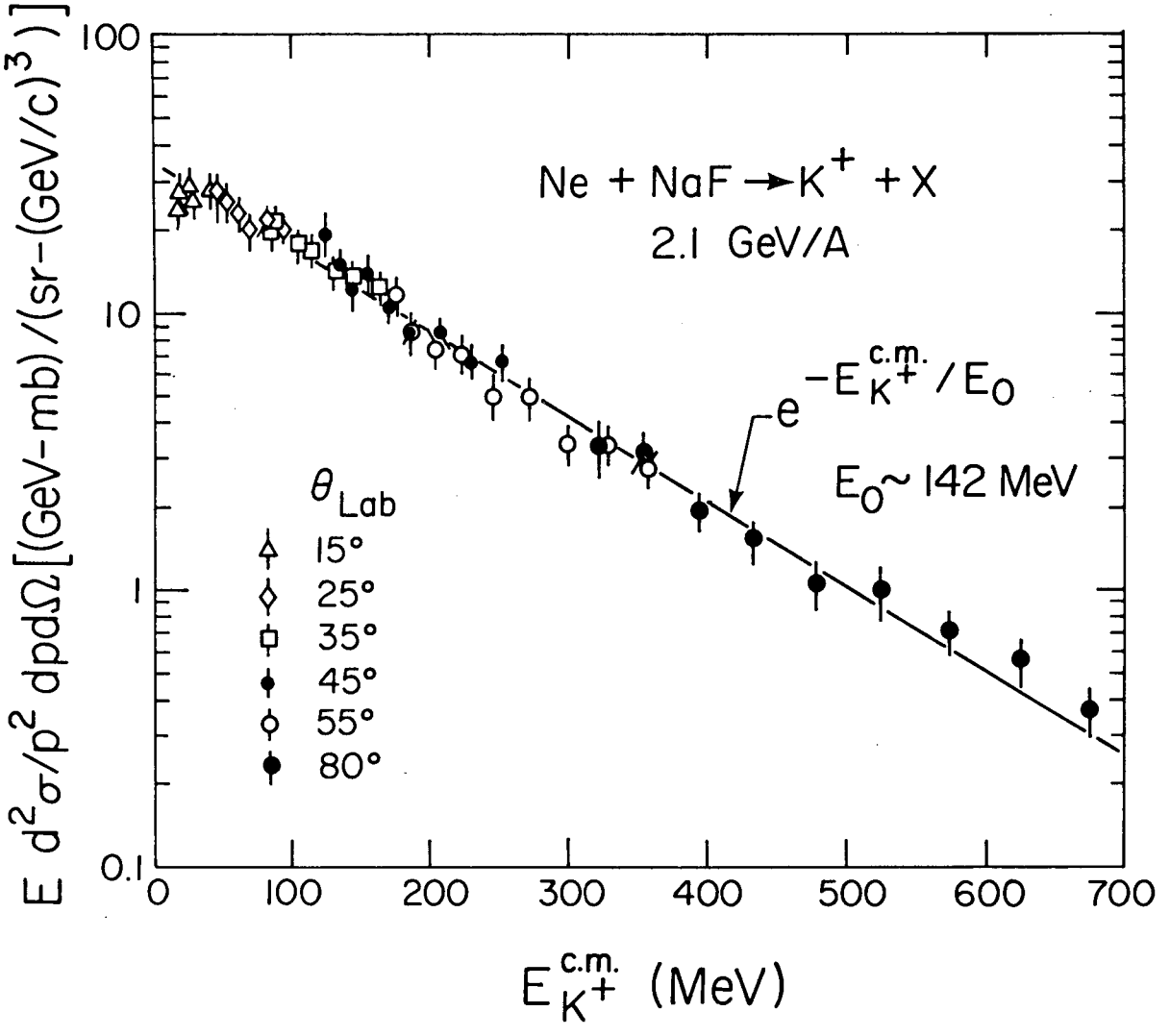

XBL816-2361

Fig. 5

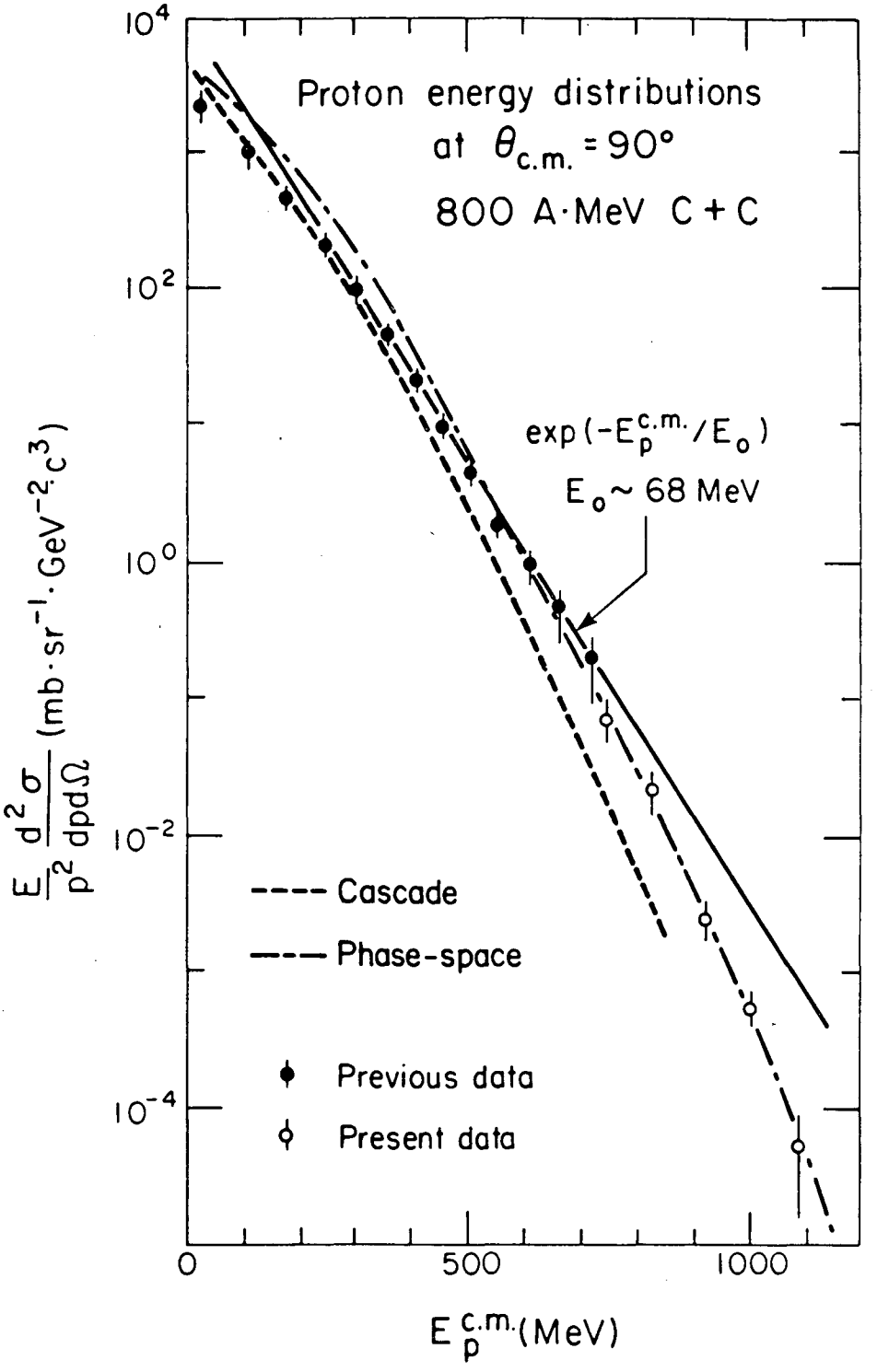

XBL 839-872A

Fig. 6

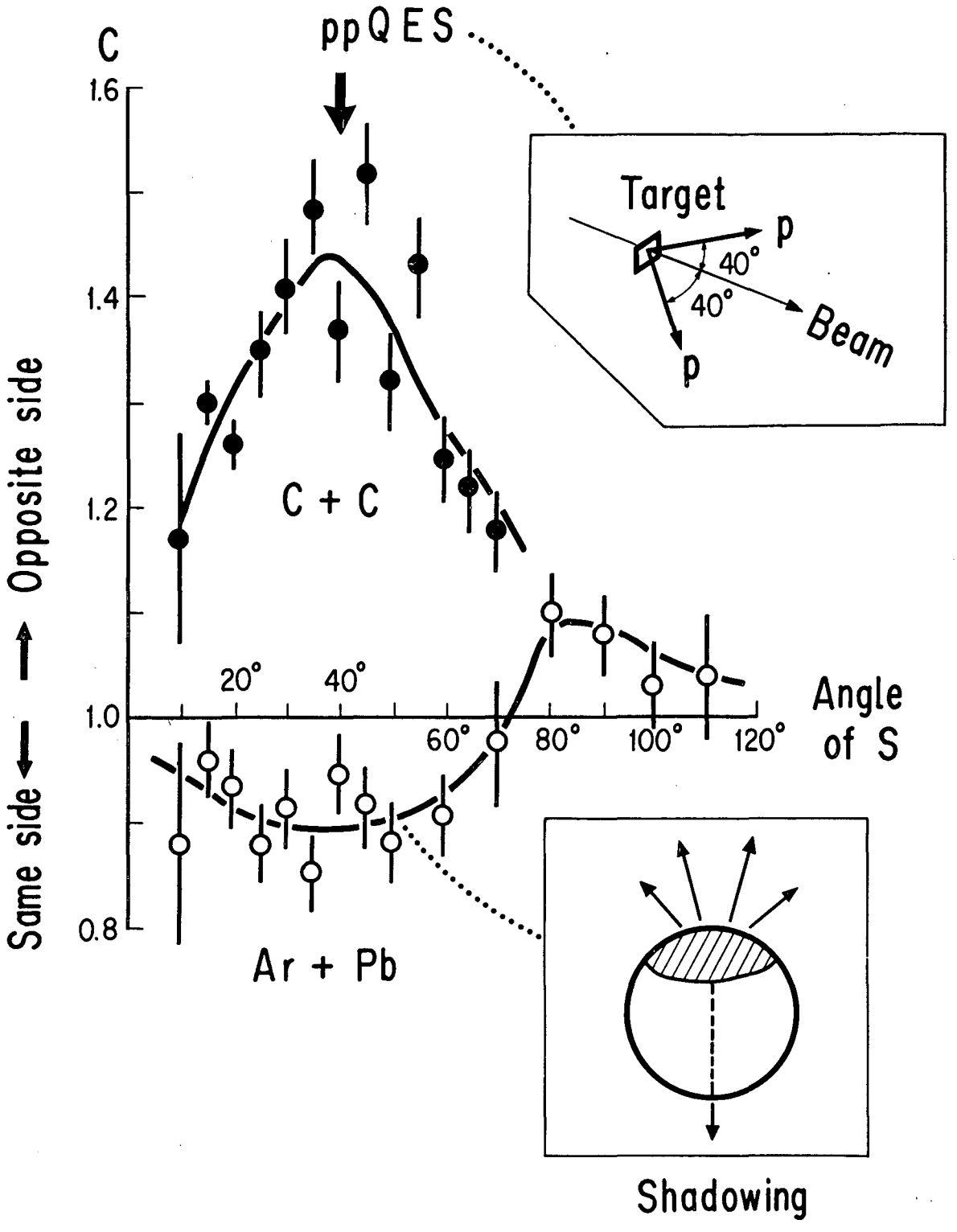

XBL 841-285

Fig. 7

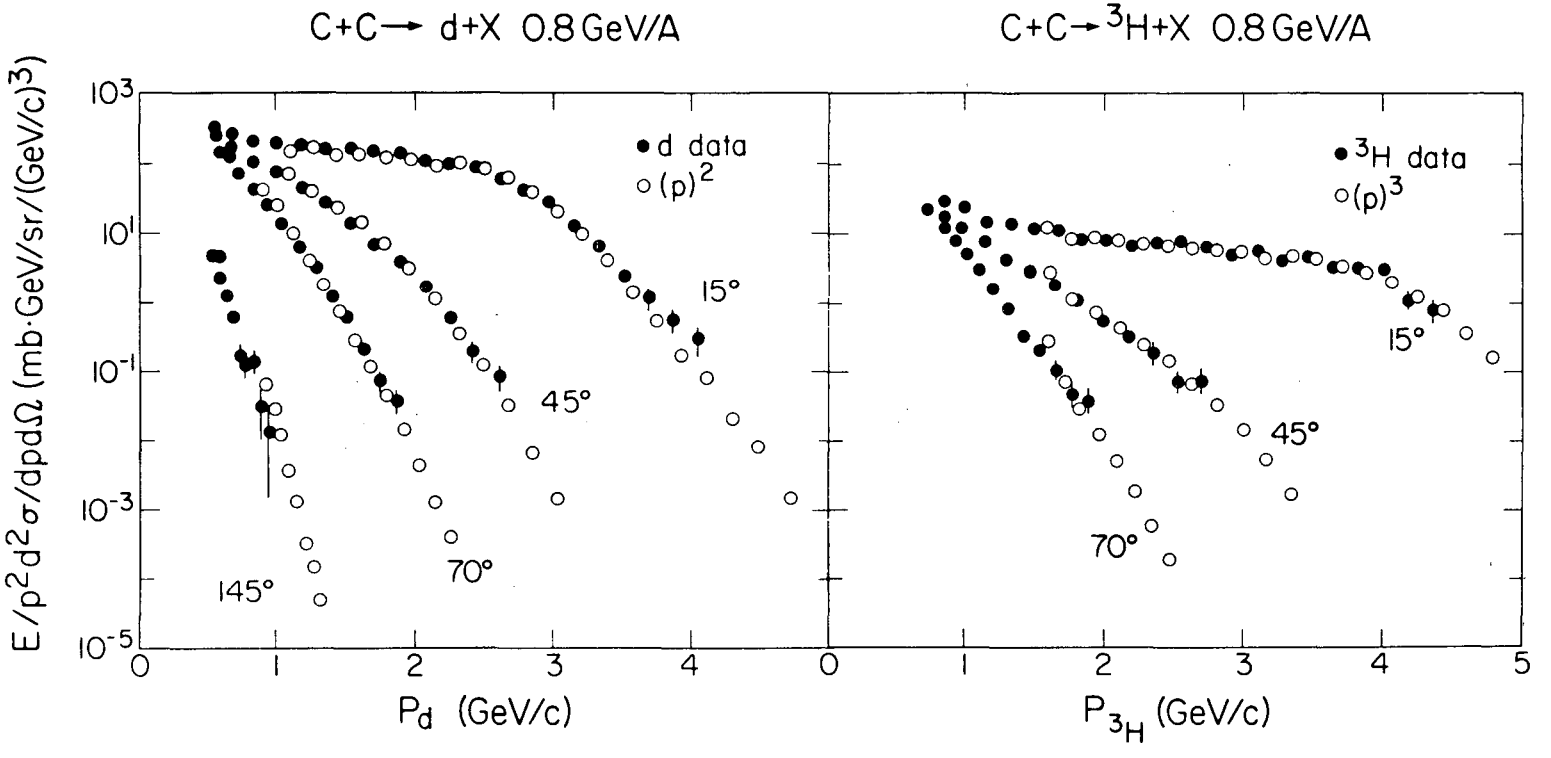
C+C→ d+X 0.8 GeV/A
C+C→ ^{3}H+X 0.8 GeV/A
$E/p^2 d^2\sigma/dpd\Omega$ (mb·GeV/sr/(GeV/c)^3)
10^3
10^1
10^{-1}
10^{-3}
10^{-5}
● d data
○ $(p)^2$
● ^{3}H data
○ $(p)^3$
15°
45°
70°
145°
0
1
2
3
4
5
P_d (GeV/c)
$P_{^3H}$ (GeV/c)
XBL 841-280

Fig. 8

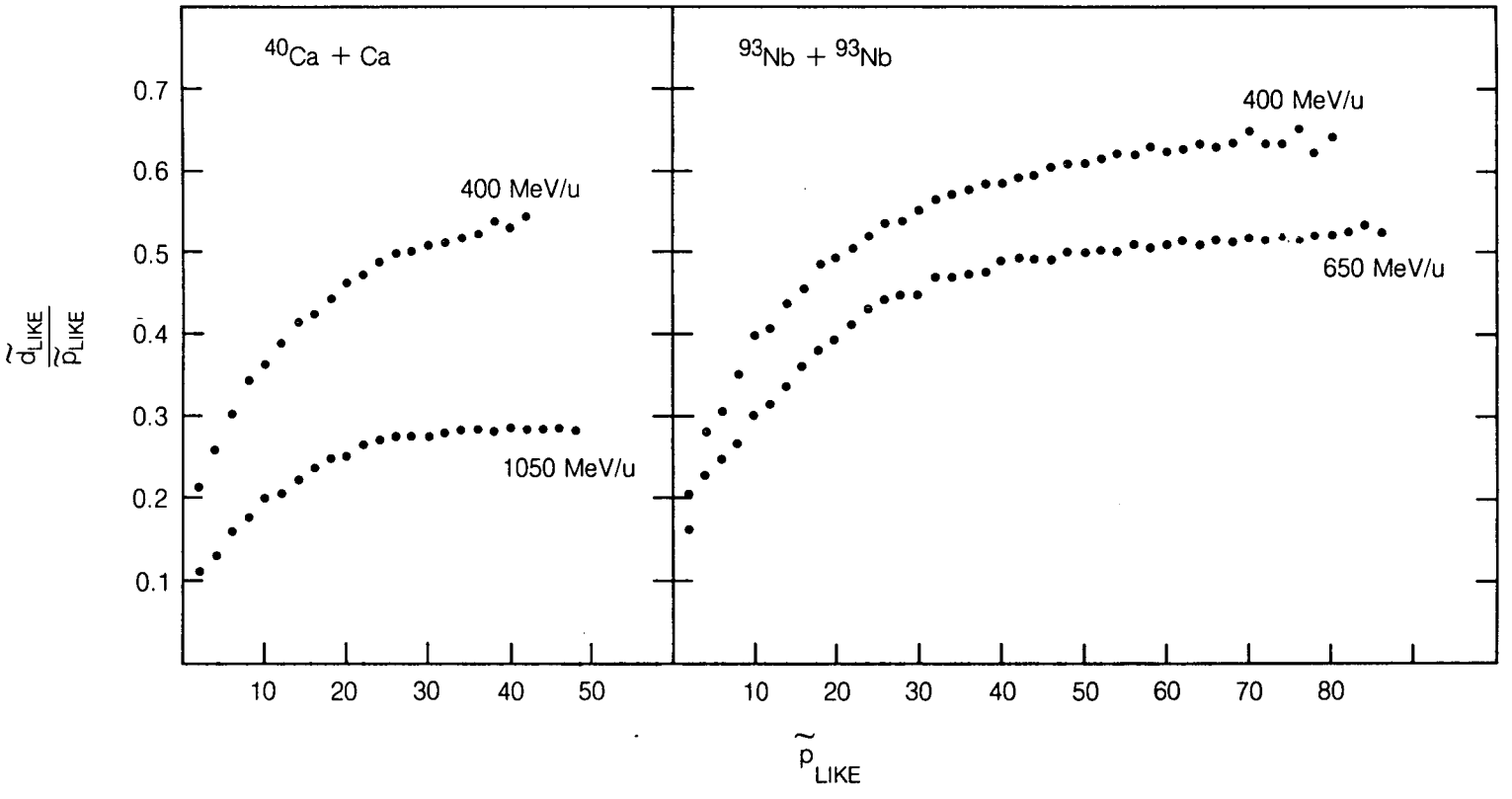
^{40}Ca + Ca
^{93}Nb + ^{93}Nb
400 MeV/u
1050 MeV/u
400 MeV/u
650 MeV/u
$\frac{\tilde{d}_{LIKE}}{\tilde{p}_{LIKE}}$
$\tilde{p}_{LIKE}$
0.1
0.2
0.3
0.4
0.5
0.6
0.7
10
20
30
40
50
60
70
80
XBL 835-247

Fig. 9

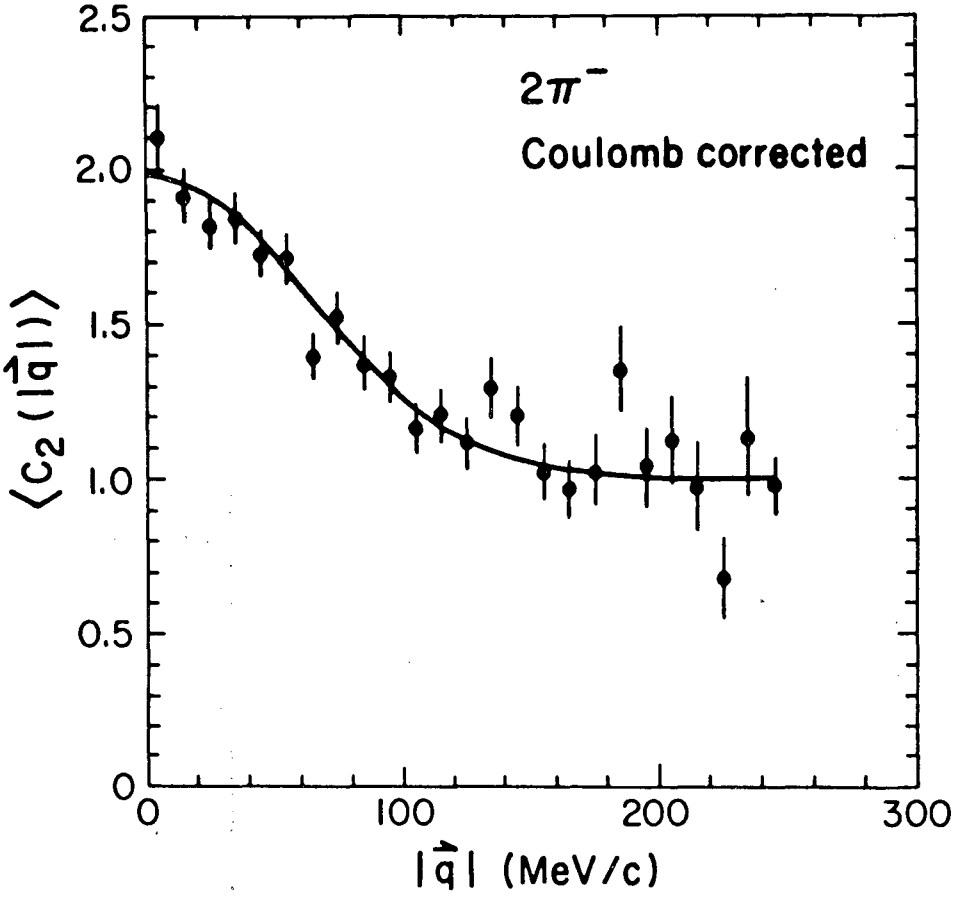

XBL 816-3219B

Fig. 10

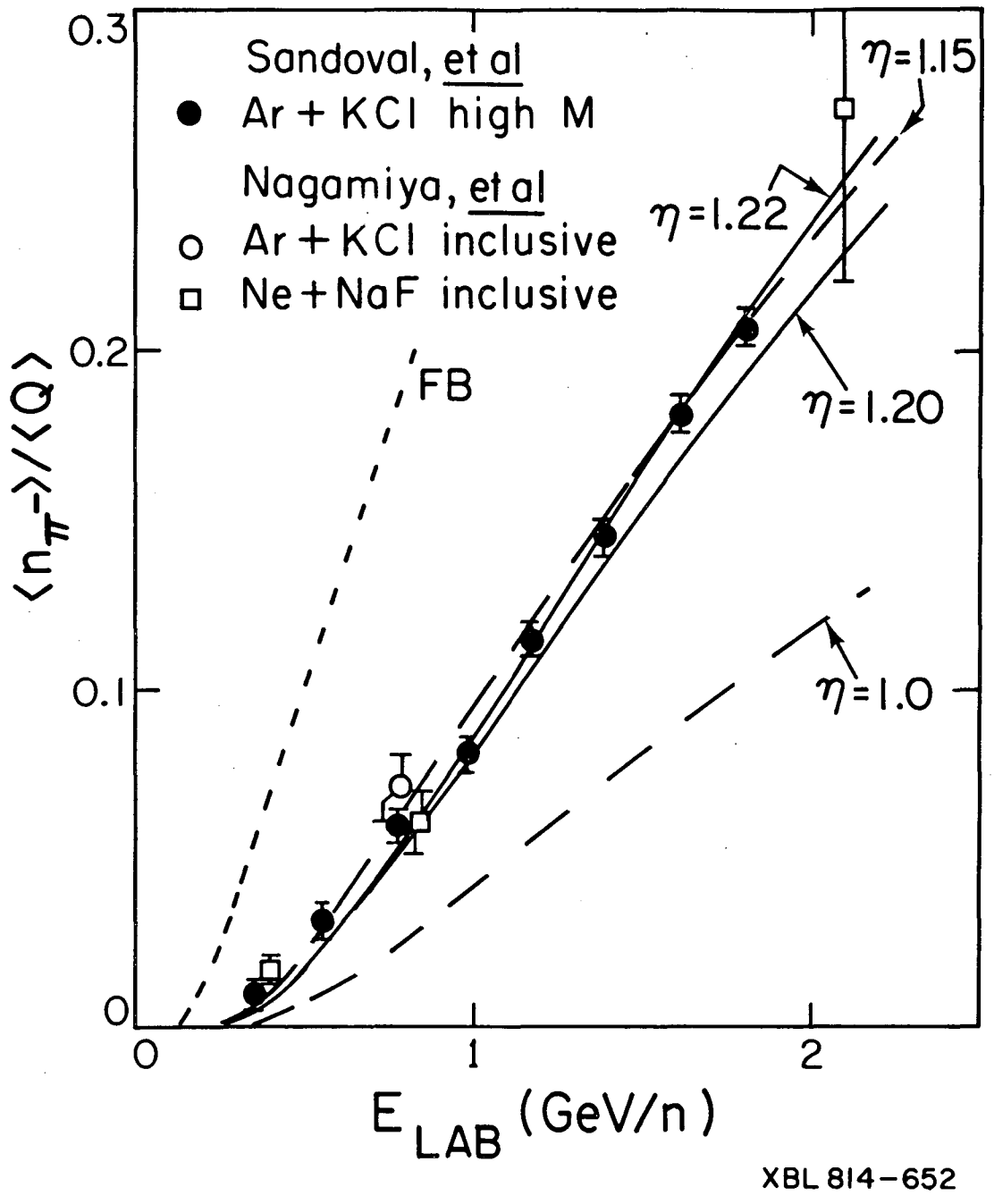
Sandoval, et al
Ar + KCl high M
Nagamiya, et al
Ar + KCl inclusive
Ne + NaF inclusive
FB
η=1.15
η=1.22
η=1.20
η=1.0
0.3
0.2
0.1
0
0
1
2
⟨nπ⁻⟩/⟨Q⟩
E LAB (GeV/n)
XBL 814-652

Fig. 11a

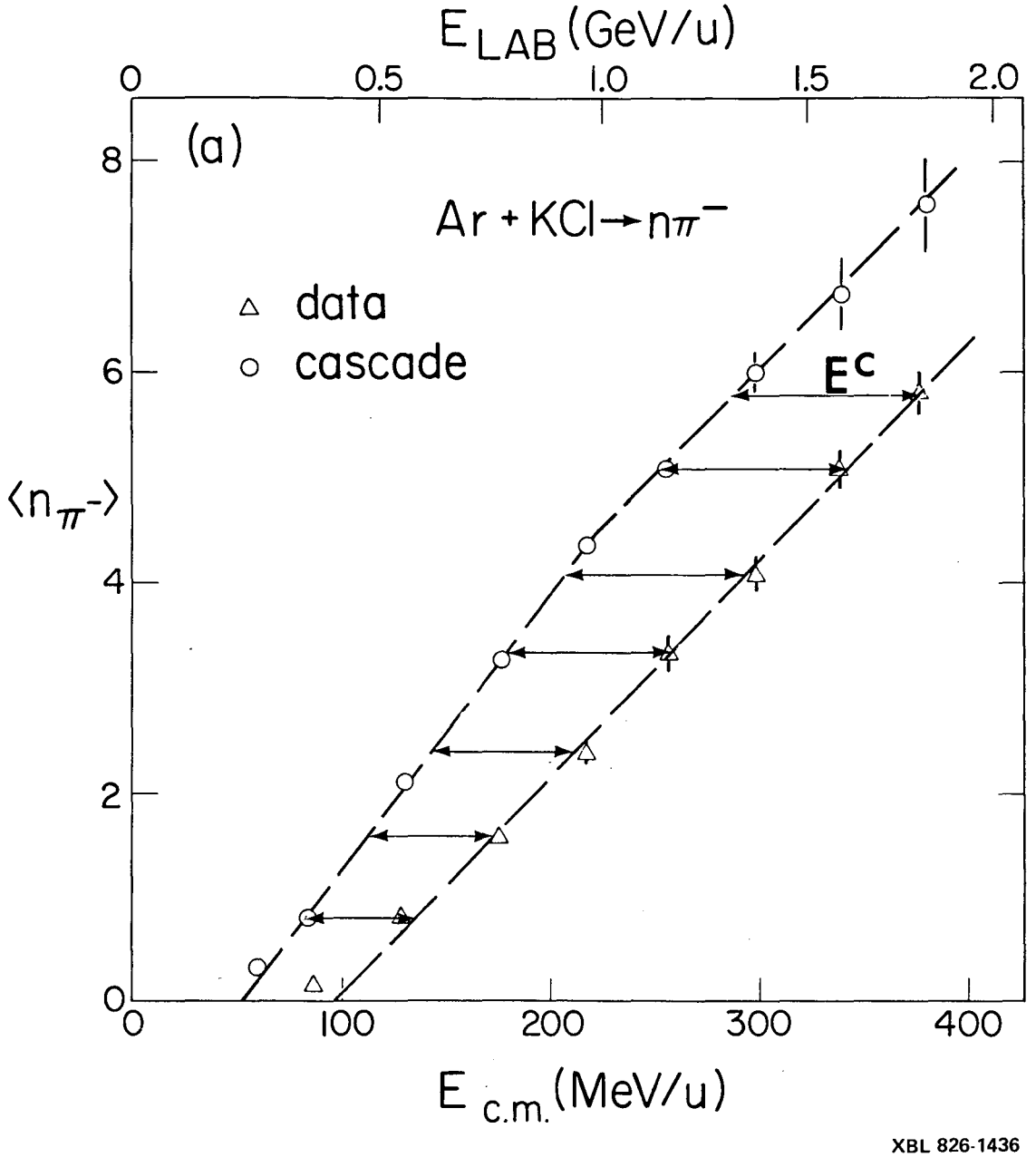
E LAB (GeV/u)
0
0.5
1.0
1.5
2.0
(a)
Ar + KCl → nπ⁻
△ data
○ cascade
E^c
⟨nπ⁻⟩
8
6
4
2
0
0
100
200
300
400
E c.m. (MeV/u)
XBL 826-1436

Fig. 11b

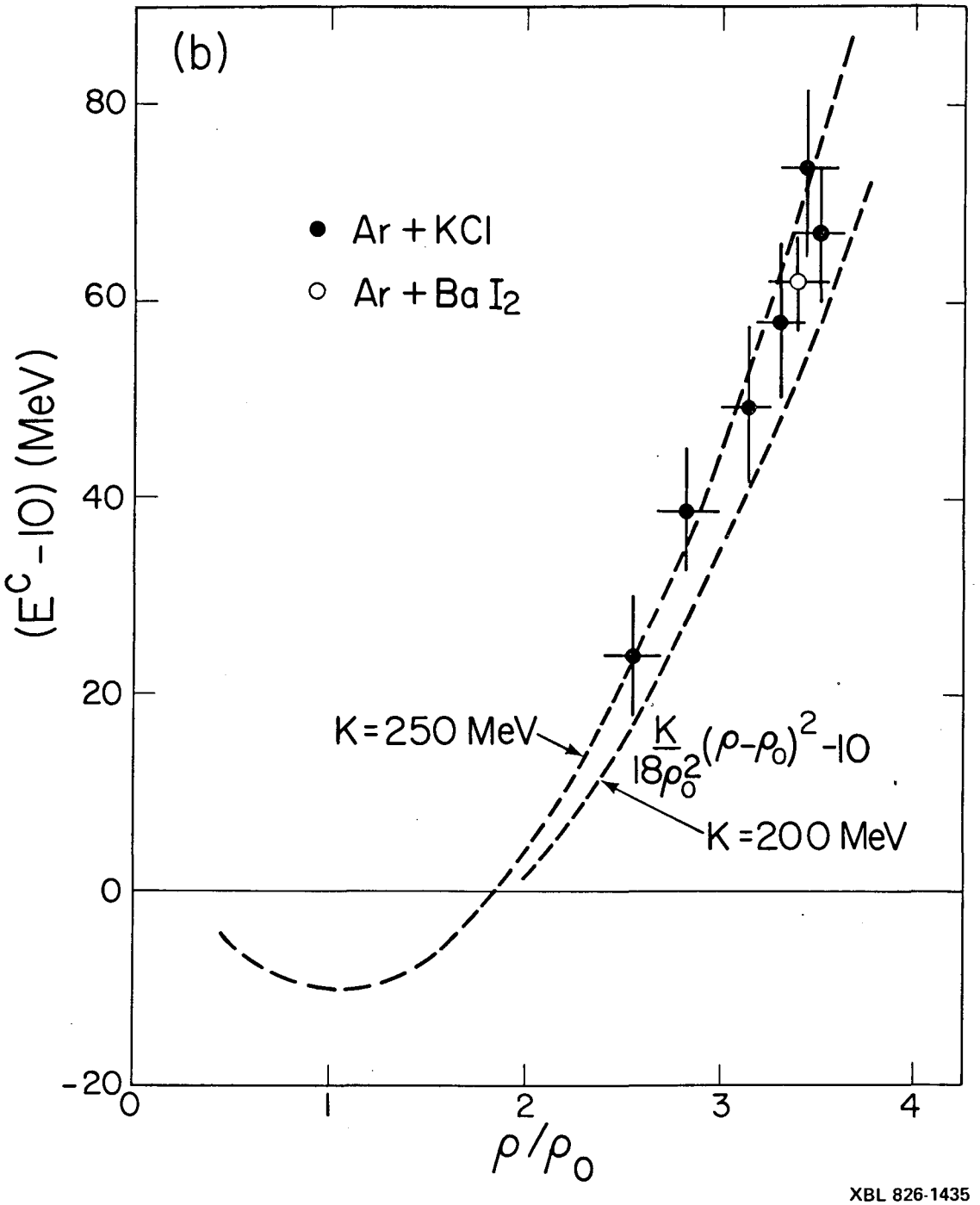
(b)
80
60
40
20
0
-20
0
1
2
3
4
$(E^c - 10)$ (MeV)
ρ/ρ_0
● Ar + KCl
○ Ar + Ba I_2
K = 250 MeV
$\frac{K}{18\rho_0^2}(\rho-\rho_0)^2 - 10$
K = 200 MeV
XBL 826-1435

Fig. 12

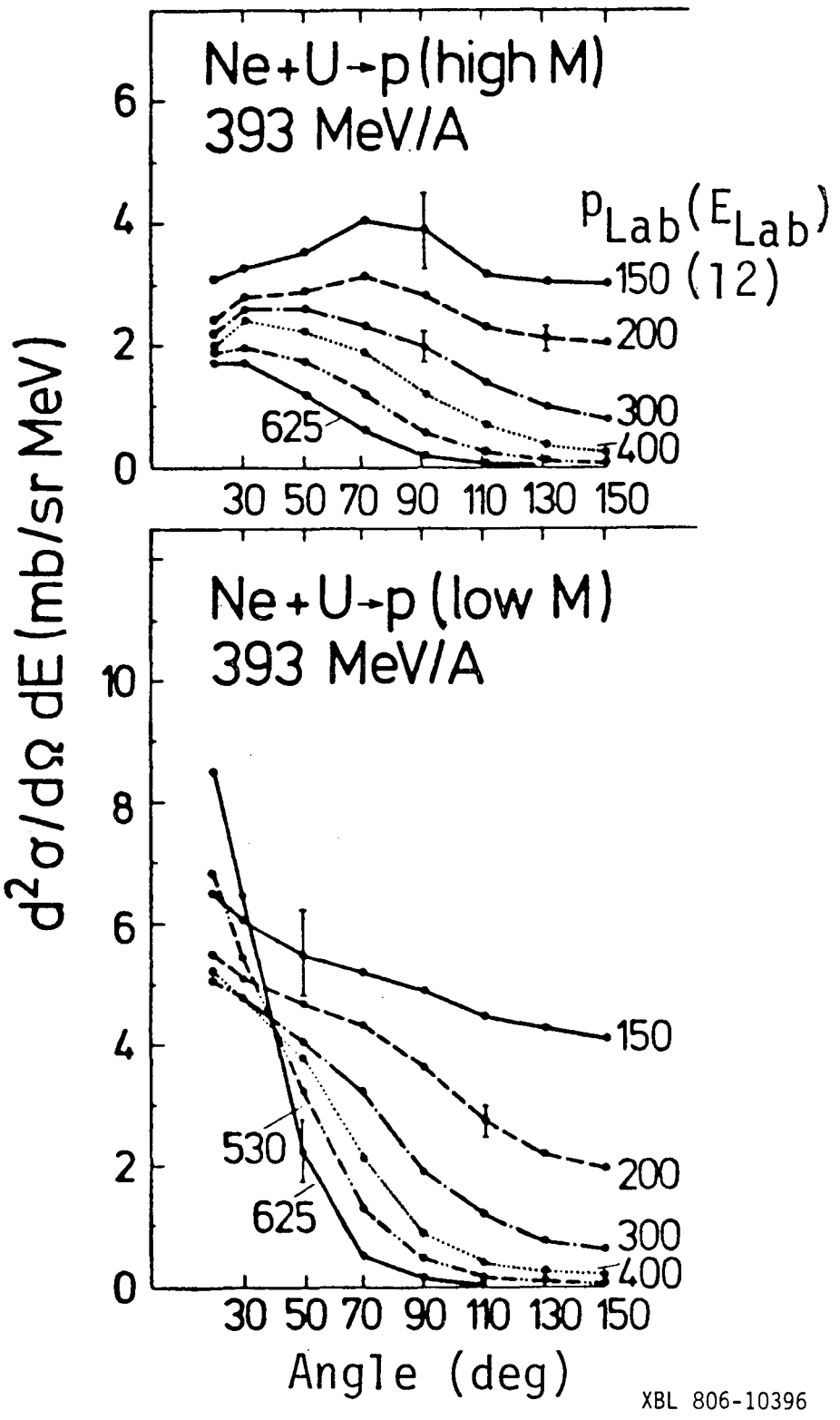
Ne+U→p (high M)
393 MeV/A
$p_{Lab}(E_{Lab})$
150 (12)
200
300
400
625
Ne+U→p (low M)
393 MeV/A
150
200
300
400
530
625
$d^2\sigma/d\Omega\, dE$ (mb/sr MeV)
Angle (deg)
XBL 806-10396

Fig. 13

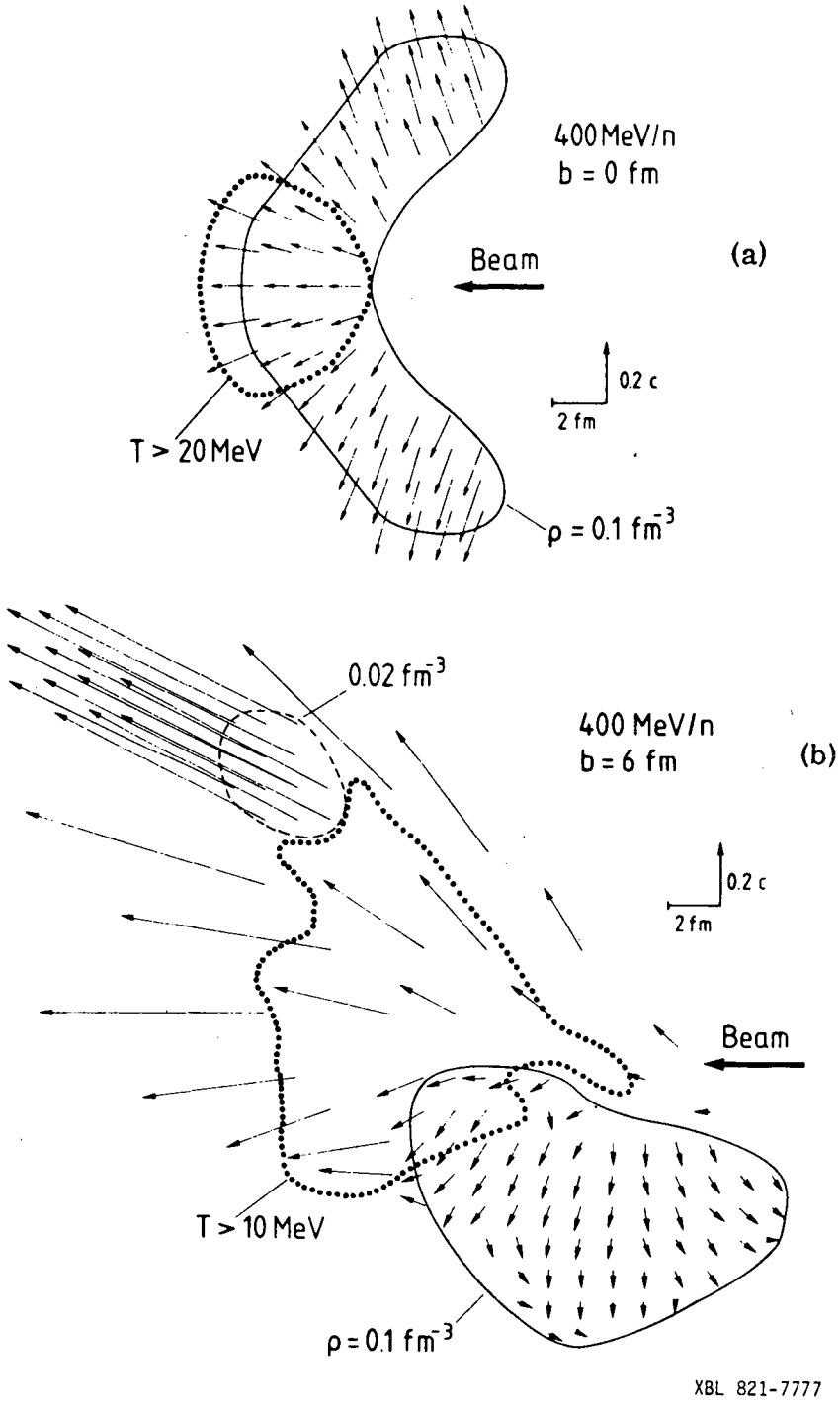
400 MeV/n
b = 0 fm
Beam
(a)
0.2 c
2 fm
T > 20 MeV
ρ = 0.1 fm⁻³
0.02 fm⁻³
400 MeV/n
b = 6 fm
(b)
0.2 c
2 fm
Beam
T > 10 MeV
ρ = 0.1 fm⁻³
XBL 821-7777

Fig. 14

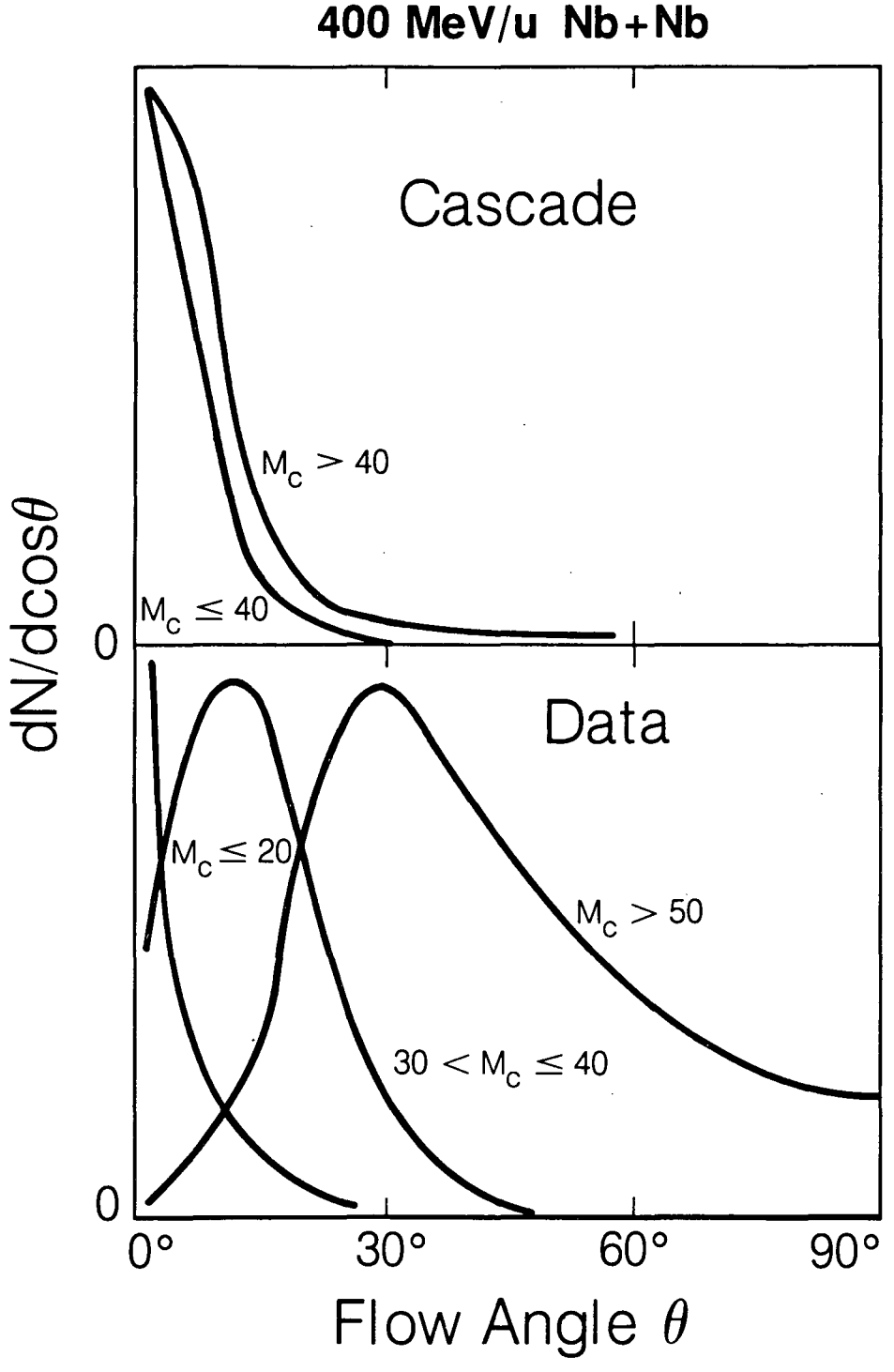

XBL 835-244

Fig. 15

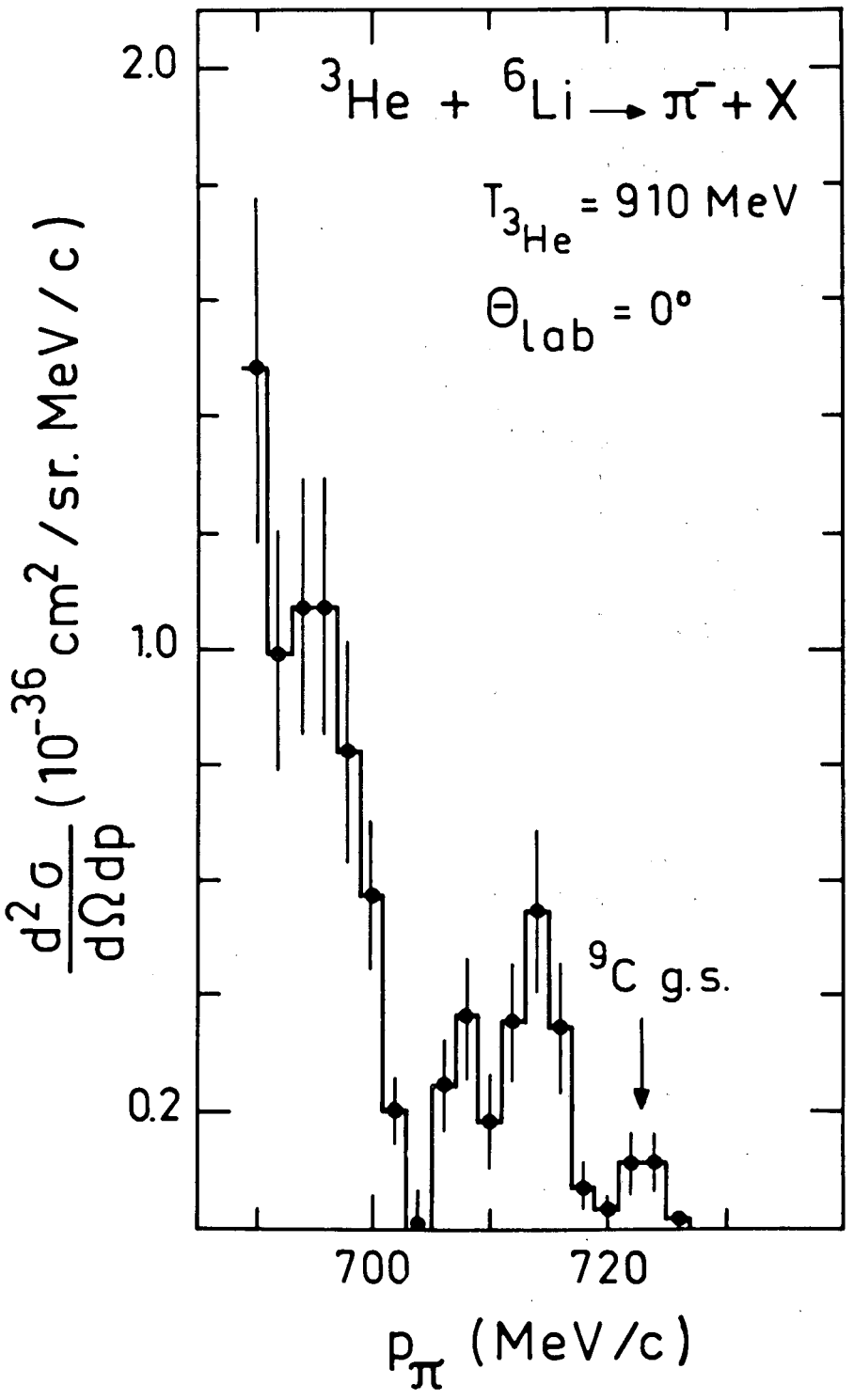

XBL 841-369

Fig. 16

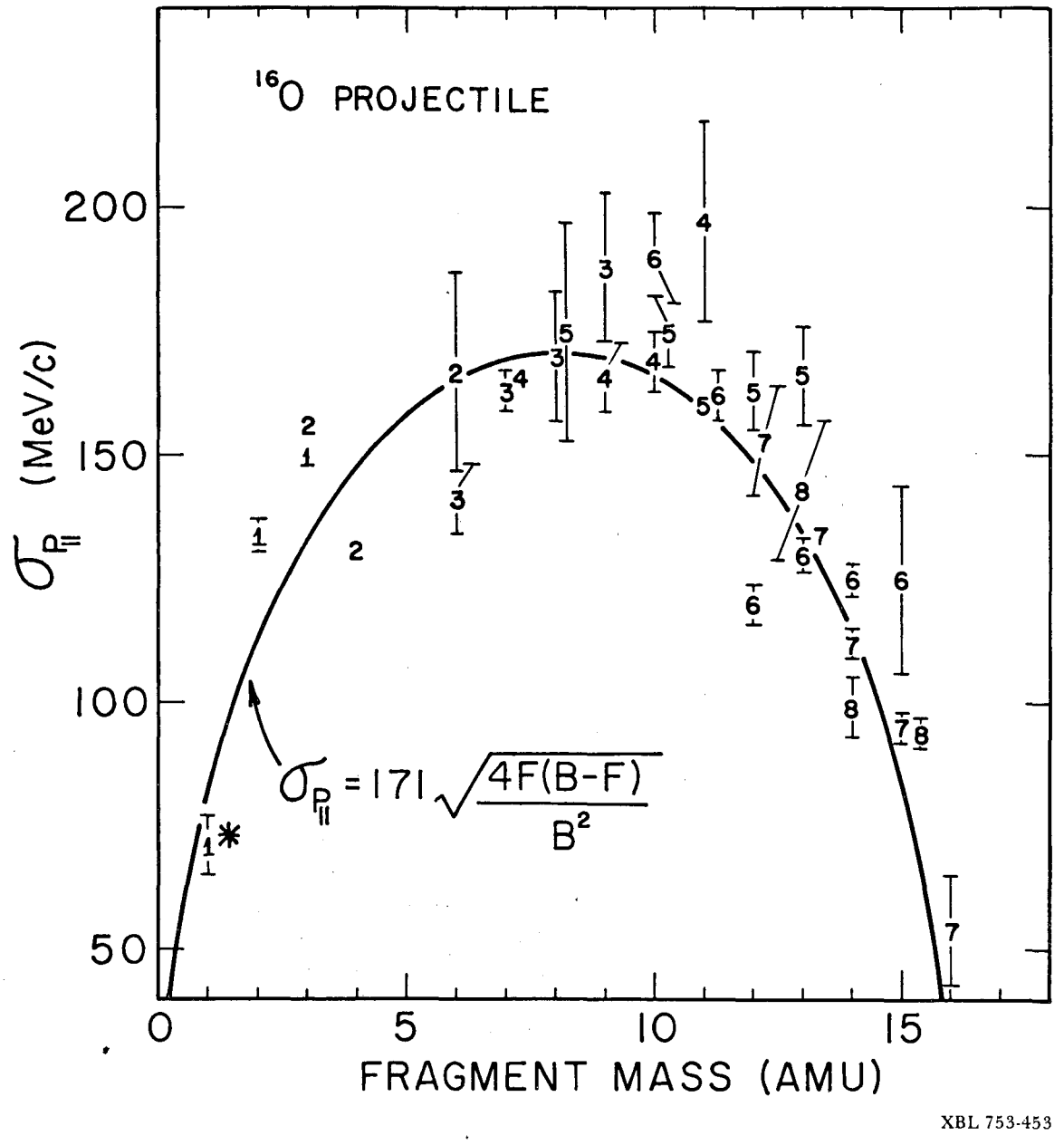
^{16}O PROJECTILE
200
150
100
50
$\sigma_{P_{\parallel}}$ (MeV/c)
0
5
10
15
FRAGMENT MASS (AMU)
$\sigma_{P_{\parallel}} = 171\sqrt{\frac{4F(B-F)}{B^2}}$
XBL 753-453

Fig. 17

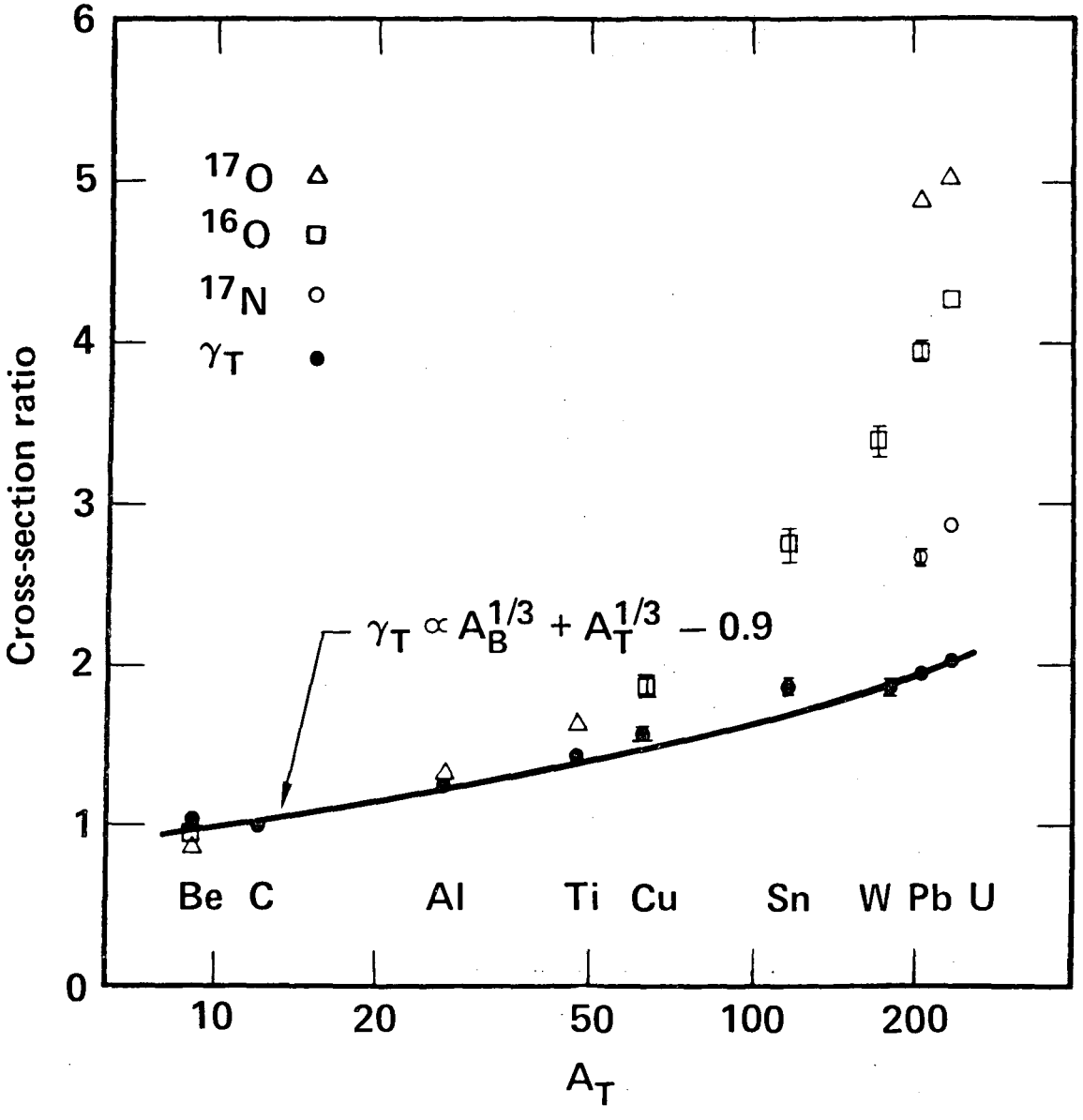

XBL 841-287

Fig. 18

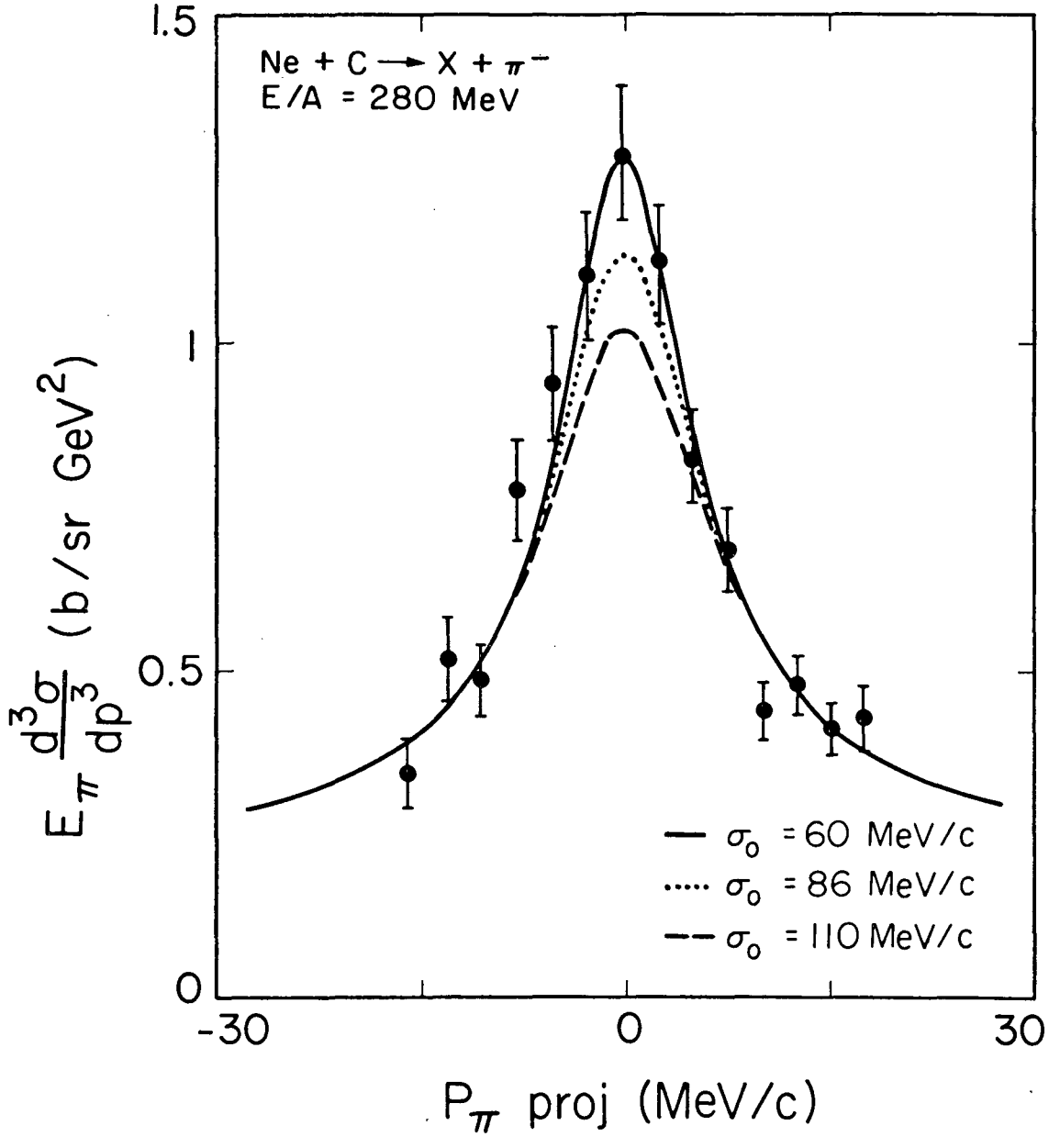

XBL816-2347

Fig. 19

TECHNICAL INFORMATION DEPARTMENT
LAWRENCE BERKELEY LABORATORY
UNIVERSITY OF CALIFORNIA
BERKELEY, CALIFORNIA 94720